The Use of Millimeter Doppler Radar Echoes to Estimate Vertical Air Velocities in the Fair-Weather Convective Boundary Layer

BART GEERTS AND QUN MIAO

University of Wyoming, Laramie, Wyoming

(Manuscript received 3 May 2004, in final form 20 August 2004)

ABSTRACT

Vertical velocity characteristics of the optically clear convective boundary layer (CBL) are examined by means of profiling airborne radar data collected in the central Great Plains during the International H_2O Project, May–June 2002 (IHOP 2002). Clear-air echoes are sufficiently strong for the radar, a 95-GHz cloud radar, to detect most of the CBL at a resolution of ~30 m. Vertical radar transects across the CBL are remarkably dominated by well-defined plumes of higher reflectivity. These echo plumes occupy most of the depth of the CBL in the developing and mature stages of the CBL. Gust probe data indicate that the plumes tend to correspond with ascending motion. Evidence exists in the literature, and arises from this study, that the clear-air scatterers are mostly small insects.

The close-range Doppler radar velocities, some 100 m above and below the aircraft, are compared to gust probe vertical velocities after both are corrected for aircraft motion.

It is found that the radar vertical velocities have a downward bias of 0.5 ± 0.2 m s^{-1} on average. This bias is of the same sign as that reported in wind profiler data in the CBL, but it is larger. The difference between aircraft and radar vertical velocities becomes larger in stronger updrafts. This does not happen in cases where the scatterers are hydrometeors: hydrometeors fall out at their terminal velocity, which does not directly depend on updraft speed.

The existence of the CBL echo plumes and radar "fine lines," sustained by low-level air convergence, has long been attributed to a biotic response to updrafts. This response has been assumed to be controlled by air temperature; that is, insects subside when they encounter cold air in the upper CBL. The authors propose that the biotic response is not temperature controlled but, rather, is dependent on the vertical displacement.

1. Introduction

In recent years cloud properties have been studied increasingly by means of millimeter-wave Doppler radars. Their short wavelength allows these radars to sense cloud droplets or ice crystals and to infer cloud-scale kinematics at high resolution (e.g., Pazmany et al. 1994: Syrett et al. 1995). These radars also record echoes in the optically clear boundary layer (e.g., Clothiaux et al. 2000), as do the operational scanning weather radars, which are centimeter wave. These clear-air echoes occur mainly in the warm season and mainly over land (Wilson et al. 1994). They are a nuisance for radar-based studies of continental boundary layer clouds since they may contaminate the true cloud echo and hide the cloud base (e.g., Martner and Moran 2001).

Corresponding author address: Dr. Bart Geerts, Department of Atmospheric Sciences, University of Wyoming, Laramie, WY 82071.
E-mail: geerts@uwyo.edu

The precise nature of shallow clear-air radar echoes remains controversial (e.g., Gossard 1990), but it is now well established that at least in the convective boundary layer (CBL) over land these echoes are largely due to particle scattering by insects rather than to refractive index gradients (Russell and Wilson 1997; Riley 1999). This is true also for "fine lines," shallow lines of echo strong enough to be seen by operational C- or S-band radar scanning just above the horizon (Wilson et al. 1994). Forecasters monitor these fine lines in the warm season because thunderstorms may be triggered along them, as has been shown by numerous studies (e.g., Wilson and Schreiber 1986; Wilson et al. 1992; Wilson and Megenhardt 1997; Koch and Ray 1997; Geerts et al. 2004, manuscript submitted to *Mon. Wea. Rev.*).

Under some circumstances Bragg scattering may dominate the echo seen by these radars, for example, along the perimeter of cumulus clouds (Knight and Miller 1993) or in an inversion, but Bragg scattering, due to refractive index turbulence in the inertial subrange, yields a return that is 55 dBZ smaller for a W-band (3 mm, 95 GHz) cloud radar than for an S-band

(10 cm, 3 GHz) radar [Eq. (A4) in Knight and Miller 1998]. Therefore, clear-air CBL echoes at millimeter wavelengths are unambiguously due to particle scattering. As will be discussed later, this scattering is believed to be largely due to microinsects (<10 mm in diameter). On the other hand, clear-air return in 915-MHz wind profilers is largely due to Bragg scattering, although in the presence of large particles such as raindrops, insects, or birds, both Bragg scattering (due to turbulence) and particle scattering contribute to the observed echo (Ecklund et al. 1988).

Radar echoes in the clear CBL are rather ubiquitous. Clothiaux et al. (2000, Fig. 12) use a sensitive, zenith-pointing 35-GHz radar to show that about 90% of the radar range gates are "contaminated" by insect clutter at 1 km above ground level (AGL) in June–August at a site in Oklahoma. This contamination in the optically clear CBL is generally less than 5 dBZ at millimeter frequencies and stronger at 35 GHz than at 95 GHz, the two most commonly used cloud radar frequencies. Yet, at both frequencies insect concentrations appear sufficient to produce an echo strength comparable to that of nonprecipitating shallow clouds and to serve as radar targets, at least in the Great Plains in the warm season (Fig. 1).

This clear-air echo strength enables cloud radars, which have a much better range and time resolution than lower-frequency radars, to document the airflow structure of the clear CBL and especially of radar fine lines. The radar velocities may be affected by insect motion (e.g., Achtemeier 1991; Wilson et al. 1994; Dean and Drake 2002). Fortunately, microinsects are weakly flying; in fact, they have been referred to as aerial plankton (Drake and Farrow 1988; Russell and Wilson 1997). They tend to move isotropically at speeds not faster than 1–2 m s^{-1} (Pedgley 1982; Pedgley et al. 1982). Their deliberate or inadvertent movement from their foraging range into the CBL will result in dispersal and migration into a new territory, but this migration is wind driven.

One outstanding puzzle in UHF wind profiler data is the tendency for average vertical motions to be negative over flat terrain, especially in the lower troposphere (Carter et al. 1995; Lothon et al. 2002). Angevine (1997) finds a long-term average downward bias of 0.1–0.3 m s^{-1} in the warm season and during daytime. His work is based on two 915-MHz wind profilers located in Illinois and Wisconsin. The bias peaks when the CBL is best developed, between about 1100 and 1500 local time (LT), and it is weaker when the prevailing wind is stronger. Lothon et al. (2002, their Fig. 8) use profiler data near local noon for 11 summer days in France to conclude that the downward bias averages 0.22 m s^{-1} at midlevels in the CBL. The bias is clearly confined to the depth of the CBL.

Such a bias can be due to hydrometeors (Ralph

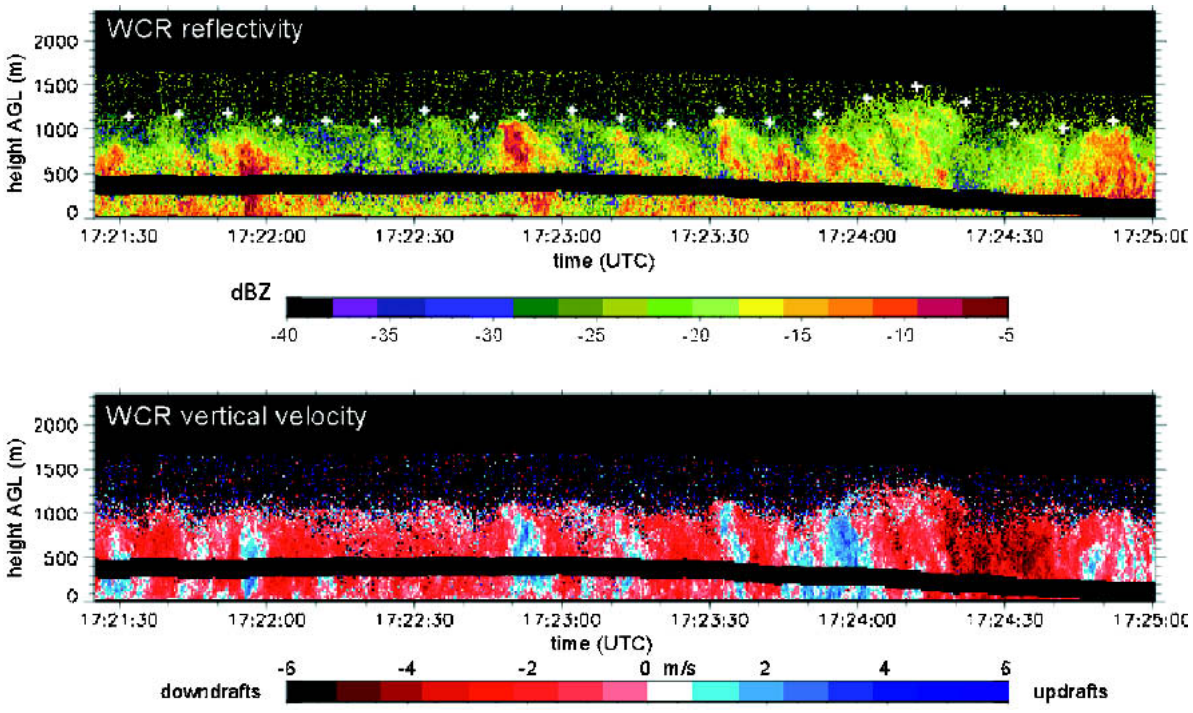

FIG. 1. Example of WCR (top) reflectivities and (bottom) vertical velocities for part of a flight leg through the CBL. One minute corresponds to roughly 5 km, so the aspect ratio of both images is about 2:1. White stars in the top panel indicate WCR-determined CBL depths (z_{i_WCR}). The 200-m blind zone contains the aircraft track. The data were collected on 29 May along the western track.

1995), gravity waves (Nastrom and VanZandt 1996), or slight antenna-pointing errors (Huaman and Balsley 1996). After assessing these explanations, Angevine (1997) discards them and suggests that the low-level radar targets (mostly particulates) have a small fall velocity. Another explanation, by Lothon et al. (2002), is that for a vertical 915-MHz beam a nonzero correlation may exist between radial velocity and refractive index fluctuations in the Doppler spectrum. Finally, Worthington et al. (2001) and Worthington (2003) suggest that the bias is due to the unfortunate and coincidental siting of wind profilers in the context of thermally direct, geographically fixed mesoscale circulations that are controlled by the topography or land surface, for instance in the vicinity of (but not on) a topographic ridge or a mountain or near (but not in) a city. Characteristics that these circulations have in common with the downward bias include a confinement to the depth of the CBL and a strong diurnal modulation. The downward vertical velocity bias in the clear CBL is not unique to wind profilers; profiling 35-GHz cloud radars (Martner and Moran 2001, Fig. 4) and C-band radars (Lothon et al. 2002) document it as well.

This study is based on an airborne Doppler cloud radar with antennas pointing up and down. Our objectives are to examine the existence of a downward Doppler velocity bias in the fair-weather CBL, to determine the cause of this bias, and, if the bias has some predictability, to improve radar-based estimates of vertical air motion in the CBL. In a follow-up study (in preparation) we use radar velocities, improved based on the results of the present study, to describe vertical air velocity patterns in the CBL and to relate these to reflectivity and flight-level buoyancy measurements, as the basis of a description of the dynamical properties of the CBL in different conditions of ambient shear.

The strength of the airborne observations, compared to ground-based radar profiles, lies in the ability to locally compare vertical air velocities to radar Doppler velocities: the aircraft carries both nadir and zenith radar antennas, and the nearest-gate Doppler velocities below and above the aircraft can be compared directly to the gust probe measurements after correction for aircraft motion. The gust probe measures air motion at a frequency similar to that of the radar. Other benefits of airborne measurements include the availability of in situ thermodynamic observations and the quasi-instantaneous measurement of the 2D (vertical and along track) echo structure.

The data sources are described in section 2, with a focus on the accuracy of radar-inferred and gust probe vertical velocities. Section 3 assesses whether and how vertical air velocity can be estimated from Doppler velocity in the fair-weather, cloud-free CBL. The results are interpreted and the observed CBL echo variability is explained in terms of speculated insect flight behavior in section 4.

2. Airborne W-band echoes and radial velocities in the clear-air convective boundary layer

a. Data collection

Some 30 h of combined radar and in situ data were collected aboard the Wyoming King Air (WKA) in the undisturbed, mature CBL over the central Great Plains of North America in May–June 2002, as part of the International H_2O Project (IHOP 2002) (Weckwerth et al. 2004). Flight levels varied from 60 m AGL to a few hundred meters above the CBL. Aircraft soundings from a few tens of meters above the ground to about 500 m above the CBL top were conducted at least 3 times during each flight, and some flights were supported by global positioning system (GPS) upsondes released along the flight track. The data shown here mainly come from flights along one of three fixed tracks, each about 60 km long (Fig. 2). A track was flown 12–18 times in either direction during a single flight, mostly between 1100 and 1600 LT (LeMone et al. 2003). The "western track" is oriented north–south in the Oklahoma Panhandle and covers pasture and scattered winter wheat fields. This land is very flat except for the Beaver Creek valley, which dips about 60 m below the plain. The "central track" is east–west oriented in south-central Kansas, covering equally flat terrain of mostly green pastures. The "eastern track" is located about 100 km east of the second track. It contained slightly undulating land of pastures and crops with a topographic ridge near the east end.

The radar used here, the Wyoming cloud radar (WCR), is a 3-mm (95 GHz) multiantenna Doppler radar (Pazmany et al. 1994; see the archival Web site at http://atmos.uwyo.edu/wcr/ for details). The key radar configuration used for this study is the *profiling* mode with fixed antennas looking up and down from the aircraft. The gate spacing is 30 m, and the first reliable radar gates are centered at 120 m (nadir) and 105 m (zenith) from the aircraft, resulting in an ~200 m blind zone, approximately centered at flight level.

b. Echo plumes

Most millimeter-wave radar scatterers in the clear CBL are believed to be microinsects. This appears to be the case for precipitation radars (3–10-cm wavelength, X to S band) (Russell and Wilson 1997); thus it should be a fortiori true for shorter-wavelength radars, such as the WCR. The reason is not merely the relative abundance of microinsects over macroinsects (>10 mm in diameter), but also because the ratio of the scattering efficiency at W band to that at S band is larger for microinsects (<10 mm) than for macroinsects (>10 mm). The scattering efficiency is the ratio of the scattering cross section to the physical cross section.

An experimental relationship between scattering cross section and insect mass has been compared to the theoretical scattering efficiency of spherical water drop-

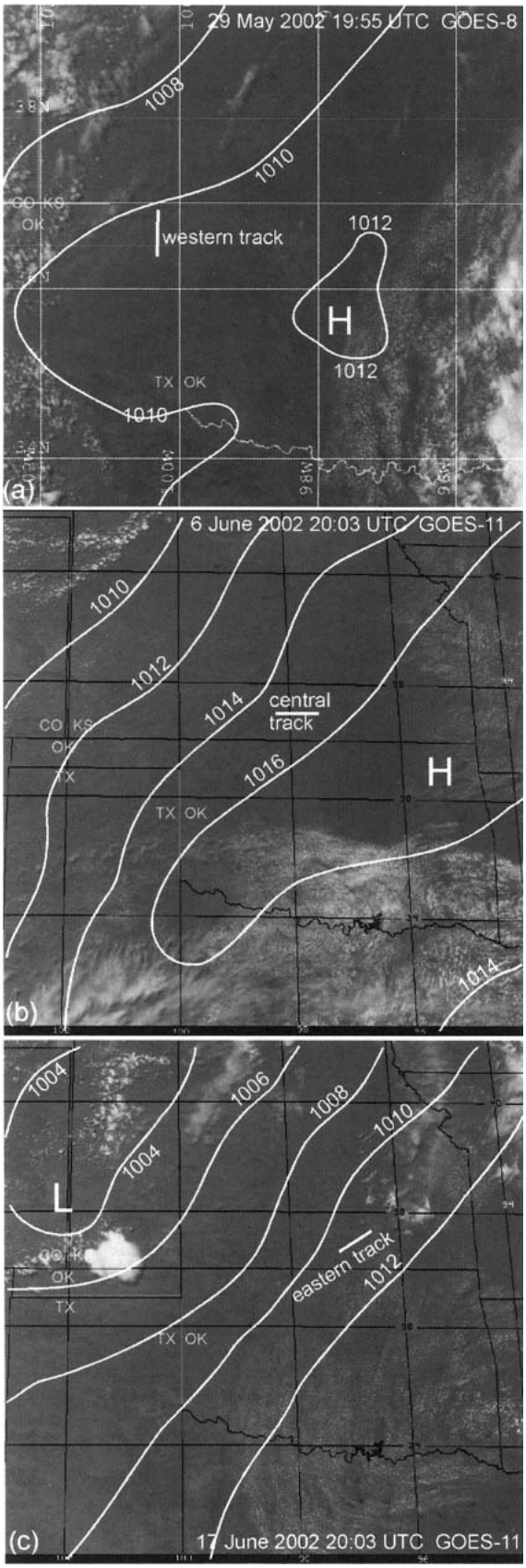

lets (Fig. 4 of Riley 1985 and Fig. 4 of Russell and Wilson 1997). This relationship shows that at X band (3 cm) the scattering efficiency increases with about the fourth power of size for insects lighter than about 100 mg (microinsects); in other words, such small insects scatter similarly to water droplets in the Rayleigh regime, which applies when the scatterers are much smaller than the radar wavelength. In the Rayleigh regime, the scattering cross section is very small for particles with a small diameter D but is proportional to D^6. Macroinsects are in the Mie regime at X band: their scattering efficiency changes little with size. For a 3-mm radar, the insect size that marks the boundary between Rayleigh and Mie is 10 times smaller, ~1 mm (0.1–1 mg in weight). Some insect species weigh less than 1 mg and are W-band Raleigh scatterers, but most of the insects that contribute to the WCR-detected echoes in the CBL (as in Fig. 1) have a Mie scattering efficiency close to unity. On the other hand, at S band all microinsects, and even the smaller macroinsects, are in the Raleigh regime and have a lower scattering efficiency.

Further evidence that the clear-air echoes are mainly weakly flying microinsects arises in section 3 below. We now examine the structure of W-band echoes in the fair-weather CBL.

1) Echo vertical structure

Our initial focus in the IHOP 2002 campaign was on mesoscale regions of low-level convergence where we aimed to document the vertical structure of radar fine lines. Yet echo plumes were generally detectable by the WCR away from radar fine lines. The study presented here is largely based on CBL observations under synoptically quiescent conditions, that is, well ahead of or before the passage of a front and distant from a dryline. The skies were generally clear (Fig. 2), allowing for strong insolation and large heat fluxes at the surface and yielding a well-developed CBL. The three days examined here have weak to moderate winds at all flight levels with no evidence of horizontal convective rolls in visible satellite or operational radar reflectivity imagery.

In the transect shown in Fig. 1, and on most other flights, the echoes are generally strong enough to describe the vertical velocity structure within the quiescent CBL. However, echoes are often close to the minimum detectable signal, and separating noise from the signal is not trivial. In terms of equivalent reflectivity, the noise increases with the square of the radar range. This is because the noise is in units of power, and the

←

FIG. 2. GOES visible satellite images of the central Great Plains near 2000 UTC (1500 CDT) (a) 29 May, (b) 6 Jun, and (c) 17 Jun 2002. Also shown are the flight track locations and the 2000 UTC sea level pressure analysis.

reflectivity factor is proportional to the returned power and to the square of the range. Therefore, the WCR data analyzed here (including those shown in Fig. 1) are subjected to a simple echo detection filter: the minimum detectable reflectivity is determined by setting the minimum WCR-received power at two standard deviations above the mean system noise, which increases with the square of the range. Any data points with received power below the threshold are eliminated.

The CBL top is clearly detectable in most reflectivity transects. The WCR echo top z_{i_WCR} can be objectively identified as the level where the mean reflectivity and signal-to-noise ratio both decrease rapidly. This is shown in Fig. 1: the plus signs are the WCR-determined CBL depth values based on 10-s mean profiles. It can be seen in the figure that 1070 m $< z_{i\_\mathrm{WCR}} <$ 1410 m AGL. In the gap regions between echo plumes, z_{i_WCR} becomes less defined and sometimes falls well below the z_{i_WCR} of plumes. To ascertain that z_{i_WCR} corresponds to the CBL top, we compare it to the thermodynamically defined CBL depth (z_{i_TH}), that is, the base of a layer in which potential temperature (θ) rapidly increases and water vapor mixing ratio (q) decreases. The profiles of θ and q, measured by a radiosonde released at 1741 UTC along the flight track on 29 May 2002 (Fig. 3), show a well-mixed CBL and a well-defined CBL top near 850 m one hour before local solar noon. Another sonde released three hours later indicates that the CBL has warmed and deepened by some 150 m. The transect in Fig. 1 is about 20 km north of the 1741 UTC sounding in Fig. 3 and nearly 20 min earlier. Precise time–space matching is important in some cases, such as on 29 May. A comparison between Fig. 1 and Fig. 3 suggests that $z_{\mathrm{i\_WCR}}$ is a few hundred meters higher than z_{i_TH}. A reflectivity transect further south, over the radiosonde site, at 1740–1744 UTC, has a z_{i_WCR} between 800 and 1000 m AGL (not shown). A similar meridional slope in CBL depth along the western track on 29 May 2002 can be seen in the reflectivity transect about one hour earlier (Fig. 4): z_{i_WCR} is near 650 m at 36.5°N and some 250 m higher near 36.8°N. The reason for this slope is believed to be a soil moisture gradient (LeMone et al. 2003). Up to 80 mm of rain fell in the southern portion of the western track during the 24 h ending at 1200 UTC 28 May, resulting in saturated soils, cooler surface temperatures, and a shallower CBL in the south (Fig. 4a) than farther north (Fig. 4b).

Conditions are more uniform for three other flights, 6, 16, and 17 June 2002. Thermodynamic profiles are

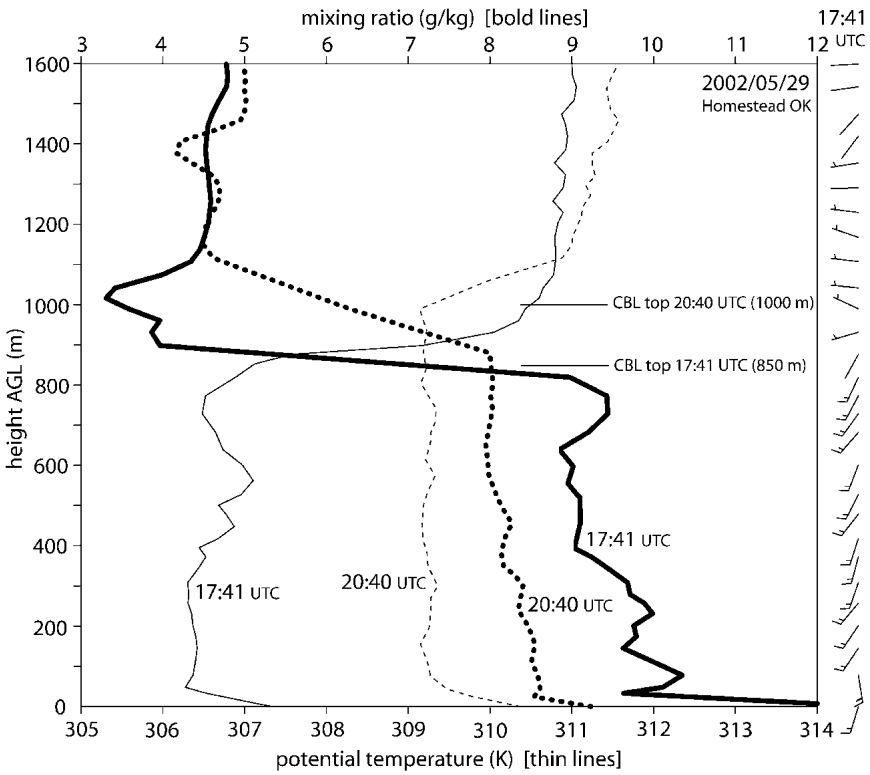

FIG. 3. Profiles of potential temperature and water vapor mixing ratio as measured by radiosondes released some 3 h apart on the western track on 29 May 2002. The lowest air temperature, just below the CBL top, is 17.8°C (18.4°C) in the 1741 UTC (2040 UTC) sounding. The profile of wind speed and direction at 1741 UTC is shown on the right (full barb: 5 m s^{-1}). The local solar noon is at 1842 UTC.

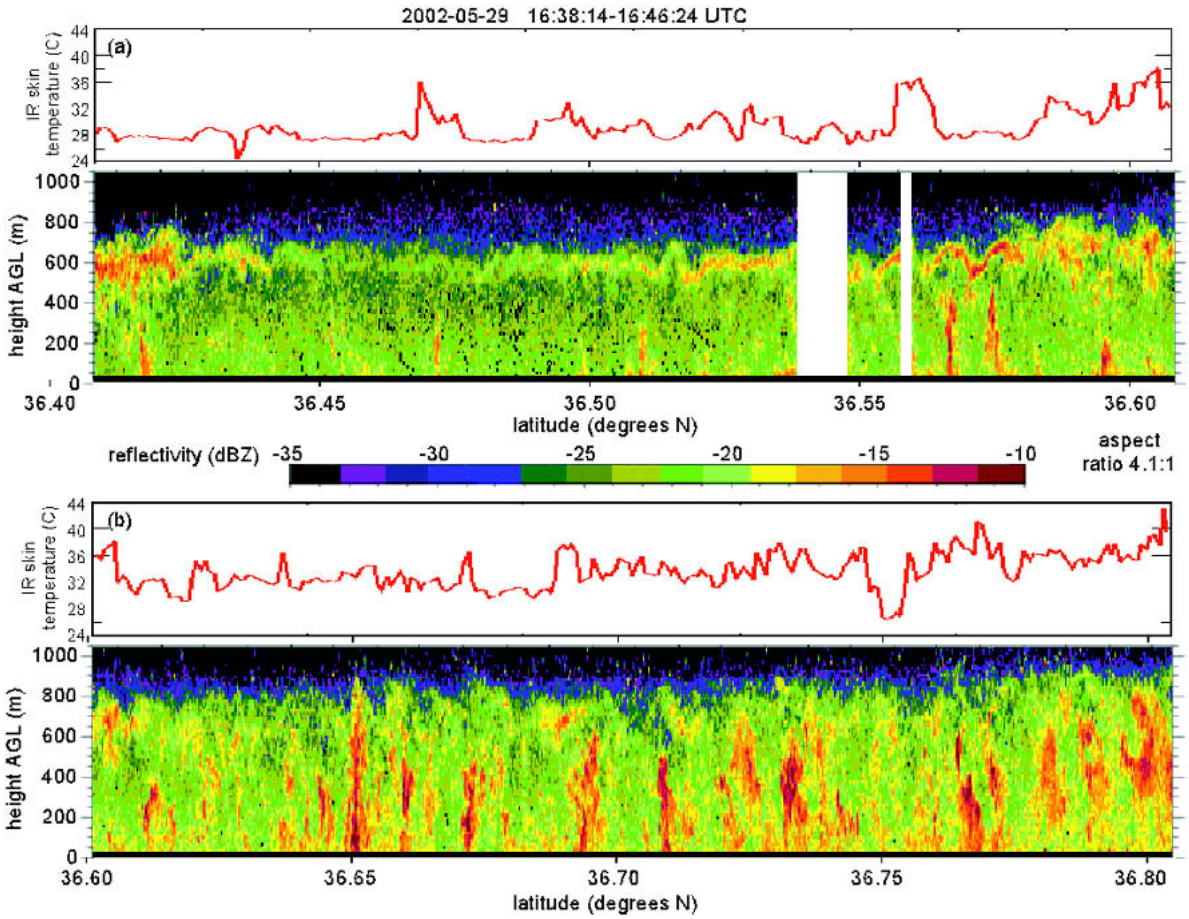

FIG. 4. Radar reflectivity transect across a boundary layer whose southern portion (a) is depressed, largely devoid of echo plumes, and marked by a weak reflectivity maximum near the top. The northern portion of this flight leg (b) has a deeper CBL and well-defined plumes. Also shown is the infrared temperature measured by a narrow-beam nadir-viewing radiometer (Heiman). At this flight level (~65 m) this temperature is a good measure of the ground temperature, which is strongly affected by soil moisture. The observations were the earliest ones collected on 29 May on the "western track." The CBL wind is from the south (left) at about 5 m s^{-1} in this transect (Fig. 3).

derived from nearby radiosondes or from aircraft sondes. The average depth z_{i_WCR} for these three cases is 1220 m and the average difference ($z_{i\_WCR} - z_{i\_TH}$) is +90 m, ranging from −30 to +220 m. This uncertainty is consistent with the variability in CBL depth, ranging from overshooting thermals to depressions in which dry, warm air from aloft may be entrained into the CBL. The z_{i_WCR} distribution is close to normal with a standard deviation σ of 100–150 m. Specifically, on 29 May, σ = 104 m while the CBL was deepening (1652–1749 UTC, N = 268), and σ = 136 when the CBL was mature (1749–1939 UTC, N = 502).

It is possible that insects sometimes concentrate near the top of the CBL or even in the stable layer above the CBL: around 1640 UTC 29 May at the southern end of the western track, a thin band of enhanced reflectivity in the upper CBL was encountered (Fig. 4). The W-band profiles do not normally reveal a band of enhanced reflectivity near the CBL top, unlike C-band and UHF profiles (Lothon et al. 2002), and the transect shown in Fig. 4 is an exception. The saturated soils at the southern end of the western track on 29 May (Fig. 4a) suppressed thermal convection and CBL depth. It is unlikely that this band of enhanced reflectivity is due to the coincident haze layer reported by the flight scientist: to produce the observed reflectivity factor of about −15 dBZ (Fig. 4a), a concentration of about 3×10^{10} m^{-3} of wetted aerosol of 10 μm in diameter is needed, which is unrealistically high. The echo is more likely caused by a higher concentration of microinsects advected into the stable capping layer from the south where soils were drier and the CBL was deeper. This layer became disturbed by thermals that developed over warmer ground farther north, and some gravity waves can be seen above echo plumes at 36.56°S (Fig. 4a).

In short, the radar-based CBL determination corresponds well with the true, thermodynamic CBL depth. This implies that microinsects are clearly trapped in the CBL and that the obvious WCR reflectivity decay at

the top of plumes (e.g., in Fig. 1) can be referred to as the CBL depth.

2) ECHO DETECTABILITY

The question remains what fraction of the CBL can be "seen" by the WCR after noise has been suppressed. The reflectivity values range between −35 and −5 dBZ in the CBL shown in Fig. 1. Clearly this is an equivalent reflectivity; that is, in the derivation from power to reflectivity it is assumed that the scatterers are spherical water droplets, which is not the case. (For simplicity the term "equivalent" is omitted.) The radar sensitivity threshold is about –27 dBZ at a range of 1 km. The data can be interpolated onto a regular grid, and the fraction of grid points with a reflectivity above the threshold can then be readily evaluated. We divide each flight track into a series of segments each 5 km long (1 min of flight, or roughly 1800 profiles). We consider a segment to be well sampled if at least 50% of its profiles (i.e., sampled at about 30 Hz) have measurable echoes over a continuous depth of 200 m within the CBL. That threshold is achieved for 72% of the segments sampled on 29 May 2002 for a threshold reflectivity of −25 dBZ and for 97% of the segments if the threshold reflectivity is −30 dBZ (Fig. 5). The latter is the more appropriate minimum detectable signal since most CBL echoes occur within 1 km of the radar. Given the −30 dBZ threshold, the WCR can see the CBL in at least 80% of the profiles in half of all 5-km segments (Fig. 5). There is some day-to-day variability, and the echoes on the western track (as for Fig. 5) are generally weaker than those observed on the two other tracks. The implication is that, aside from the blind zone around the flight level (Fig. 1), most but not all of the CBL can be "seen" by the WCR when the aircraft flies within it.

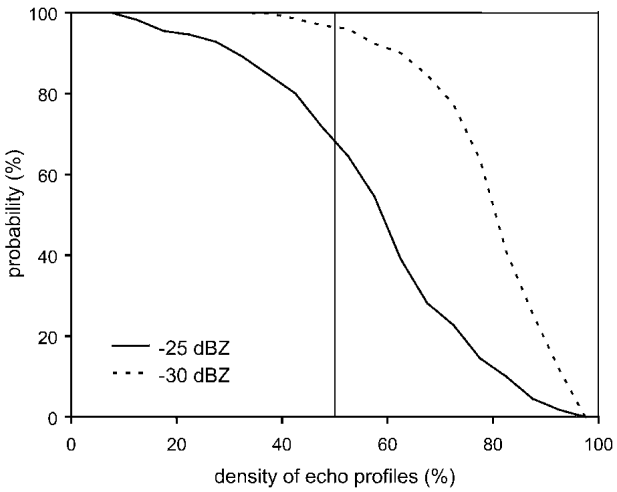

FIG. 5. Probability of encountering a density of "good" WCR echo profiles. Good profiles are defined as those with above-threshold reflectivity values over a continuous depth of at least 200 m within the CBL. Two threshold values are shown. The density of good profiles ranges from zero (none) to 100% (all) and is calculated during 1-min segments (~1800 profiles). All segments were collected during 115 min of straight and level flight legs on the afternoon of 29 May 2002 on the western track.

3) CBL ECHO VARIABILITY

The echo plumes have a maximum strength of about −10 dBZ and a height roughly corresponding to their width (Fig. 1). Most plumes cover the entire depth of the CBL. Some plumes may appear truncated simply because of wind shear normal to the transect. Three sunrise-to-noon flight datasets confirm an observation first made by Konrad (1970): echo plumes grow as the CBL deepens. An example is shown in Fig. 6, for 14 June 2002. On this day winds weaker than 5 m s^{-1} from easterly directions (roughly the same orientation as the flight track) were observed at flight level, about 380 m AGL. The plume width increases as the CBL deepens, which is consistent with observations and simulations of thermals (e.g., Barnes et al. 1980; Mason 1989). But the plumes are irregularly shaped and spaced. Some emerge from near the ground and are well defined, but have not reached the CBL top, for example, at 1530 UTC in Fig. 6. The spacing of plumes in the mature CBL generally ranges between 1 and 5 km, depending on the definition of a plume. Both the spacing and width of echo plumes, expressed as a fraction of the CBL depth, approach a lognormal distribution (not shown). The echo plumes in Figs. 1 and 6 appear cumuliform and are suggestive of thermals penetrating into a static air mass. The regions of higher insect density often have sharp upper boundaries, suggesting that upper-level divergence and diffusion are relatively slow. One notable exception is Fig. 4a, where upper-level lateral spreading appears to have occurred above a region of suppressed surface heat fluxes.

Both updrafts and downdrafts exist within plumes, but reflectivity and vertical air motion are positively correlated. This is evident from a scatterplot of gust probe vertical motion (w_a) versus WCR reflectivity (Fig. 7). The latter is displaced relative to the aircraft, but Fig. 7 shows the mean (calculated in Z units) of the first gates of the nadir and zenith beams, which is centered at flight level. Positive correlations similar to the one shown in Fig. 7 are found on all flight legs on the three days studied here (29 May, 6 and 17 June). They are stronger when the vertical velocity is filtered to eliminate wavelengths less than 200 m (the blind zone width). Echo, vertical velocity, and buoyancy characteristics of plumes will be described further in a separate study.

A large range of echo strengths exists, but on average the reflectivity decreases with height in the CBL, at a rate of about 10 dBZ km^{-1} (Fig. 8a). This suggests that more scatterers are found at low levels and/or that the low-level scatterers have a larger scattering cross section. Shown in Fig. 8a is a frequency-by-altitude diagram of radar reflectivity as measured along a flight leg

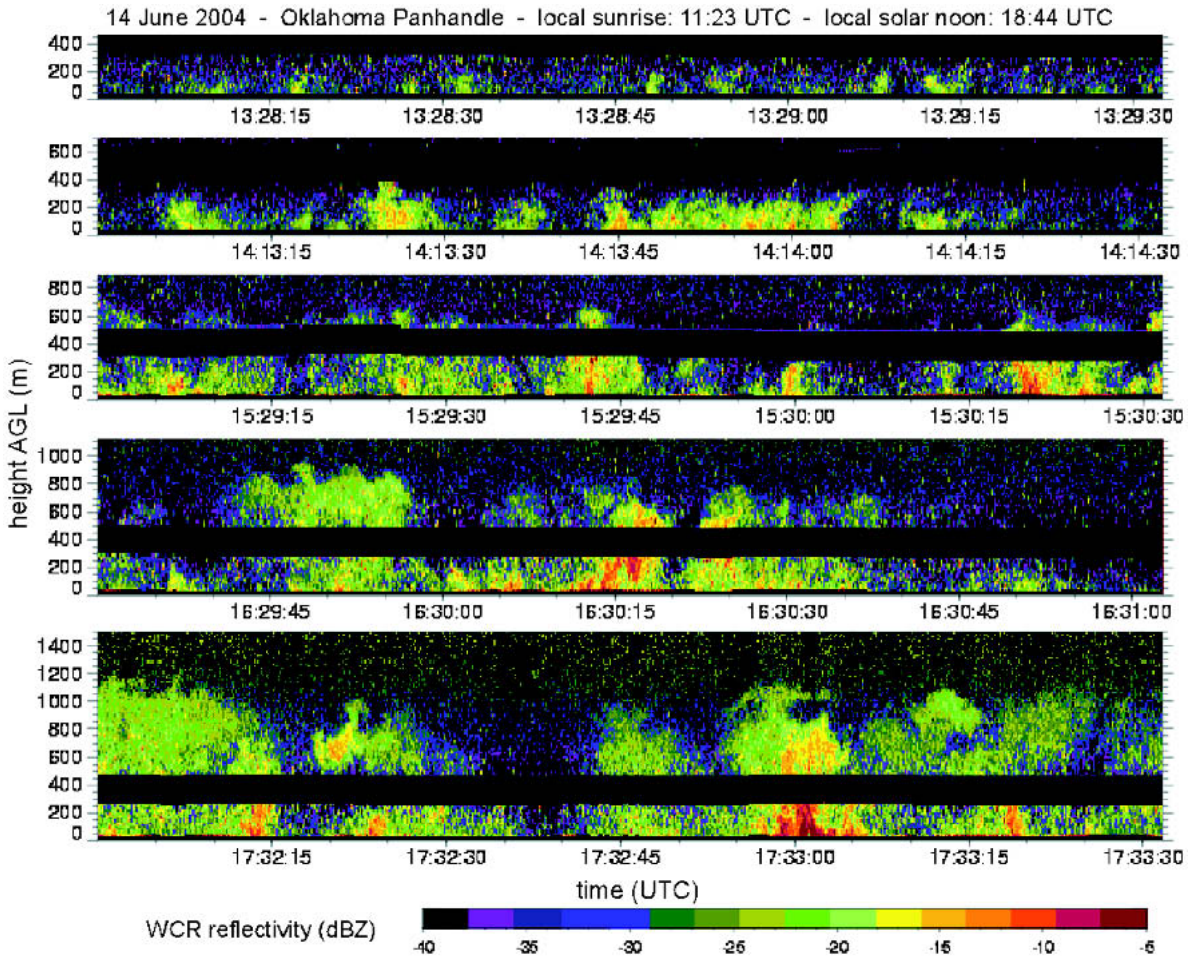

FIG. 6. WCR reflectivity transects depicting the development of the CBL on a mostly calm, mostly sunny morning over the central Great Plains on 14 Jun 2002. All cross sections have a 1:1 aspect ratio.

near 65 m AGL. This frequency is normalized; that is, the sum of all occurrences in the bins equals 100%. The most common echo strength in the upper CBL is very close to the minimum detectable signal at a range of about 1 km, so the spectrum of echo strengths is only partially detectable at large range, that is, if the flight level is low, as in Fig. 8a. The best CBL coverage is attained for flight levels near the middle of the CBL. Noise dominates the echo above the CBL, and most of this noise has been removed.

c. Accuracy of WCR vertical velocities

To infer vertical air motion from the WCR Doppler velocities, their accuracy needs to be evaluated. The echo vertical velocity, as shown in Fig. 1, is derived from the WCR radial velocities after removal of the radial velocity components due to aircraft vertical motion and departures from the exact nadir and zenith orientations due to aircraft roll and pitch (Leon et al. 1999). The aircraft motion and attitude are measured by means of an inertial navigation system (INS) and are synchronized with WCR measurements at approximately 30 Hz. For more details on WCR radial velocity processing and validation methods, see Leon and Vali (2004, manuscript submitted to *J. Atmos. Oceanic Technol.*). After correction for aircraft motion, errors are still possible because of the rapid changes in aircraft attitude and uncertainties in the exact average beam orientation. Even if the beam orientation is precisely measured, any departure from the true vertical will cause a contamination of the horizontal air velocity into the beam. Therefore, much effort was dedicated to ensuring that the nadir and zenith antennas pointed vertically.

The nadir beam orientation can be assessed by means of the mean WCR velocity at the range corresponding with the earth's surface: if the nadir antenna points forward, then the earth surface will be moving toward the radar at a fraction of the aircraft speed. That frac-

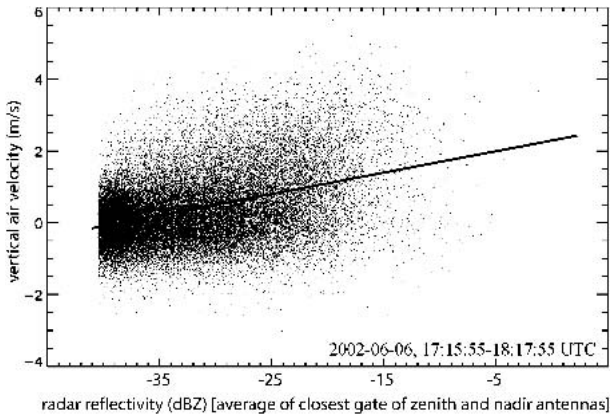

FIG. 7. A scatterplot of vertical air motion (w_a), as measured by the gust probe aboard the aircraft vs radar reflectivity for 58 min of flight data on 6 Jun 2002. The total number of observations shown is 8×10^4. The reflectivity estimate comes from just above and below the aircraft, so geometrically the average is centered at flight level.

tion is geometrically related to the offset from vertical. The average apparent velocity of the earth surface for the flights analyzed here is less than 0.10 m s^{-1} (Table 1). The average is computed for all straight and level CBL flight legs during which nadir WCR data were collected on any flight. Slight average off-vertical orientations of the nadir beam do occur during flight, depending mainly on aircraft fuel weight, but the net nadir beam velocity magnitude at the earth surface for any single flight leg is less than 0.40 m s^{-1}. The flight legs are flown in opposite directions, so the impact of the mean along-track wind on radial velocities would be cancelled. A systematic contamination of the horizontal wind into the vertical should be negligible because of the proximity of beam pointing angle to the vertical, the relatively weak CBL winds, and that the tracks were flown repeatedly in both directions.

For the zenith beam, such validation is obviously not possible, but the average nadir (w_{r_down}) and zenith (w_{r_up}) vertical velocities are within 0.30 m s^{-1} of each other (Table 1). The average zenith beam vertical velocities are slightly more negative, for all three flights. A negative bias may result from a forward displacement of the actual beam pointing angle relative to the estimated pointing angle. The average difference between zenith and nadir antennas, 0.01–0.30 m s^{-1}, is within the variability of vertical air motion over a depth of 200 m (the spacing between the up and down antenna first gates) and can also be related to height-dependent flight behavior of the scatterers within the CBL. Therefore, we did not force the average zenith beam vertical motion to equal the average nadir beam value. The implication is that w_{r_up} has an uncertainty of 0.3 m s^{-1}, while w_{r_down} has an uncertainty of at most 0.1 m s^{-1}, because of the ground validation. Thus the average of w_{r_down} and w_{r_up} has an uncertainty of 0.2 m s^{-1}.

It is not sufficient to assess mean WCR values over long flight legs. The variability of WCR-derived vertical velocity is important as well in order to address how radar vertical velocities relate to a range of vertical air motions. Therefore, we compared the spectral characteristics of the radar and gust probe vertical velocities. At scales down to ~2 s or 170 m the radar and gust probe spectra compare well, suggesting that they both capture the same eddies. At higher frequencies the power spectral density of the radar velocity decays less slowly than expected in the inertial subrange, suggesting that the high-frequency signal is affected by phenomena other than air turbulence. These include the vertical motion of scatterers relative to the air motion and radar noise. Because some of this high-frequency WCR velocity variability may be real, the WCR data were not filtered based on local velocity variability.

d. Vertical air velocities

The vertical air motion w_a is estimated at flight level from the WKA gust probe. The aircraft motion is removed from the gust probe raw winds by means of aircraft speed and acceleration obtained from the INS and aircraft attitude parameters. Because gust probe velocity components result from the integration of accelerations, their variations are known more accurately than their long-track mean. Therefore, it is customary for flux calculations to remove the long-track mean vertical velocity. The mean gust probe vertical motions for the flight legs used here (those within the CBL with both nadir and zenith WCR data), each about 12 min long, average at +0.24 m s^{-1} and range from –0.17 to +0.52 m s^{-1}. After removal of these leg averages, the resulting gust probe vertical velocity is believed to be accurate to at least 0.1 m s^{-1} (M. LeMone and A. Rodi 2004, personal communication; Lenschow 1972). Even at high frequency some uncertainty remains due to nonhydrostatic pressure variations associated with thermals. But gust probe data within the CBL capture the decay of turbulent energy in the inertial subrange well. In short, we assume an uncertainty of 0.1 m s^{-1} for the mean w_a along a flight leg, and, given the uncertainty for w_r discussed in section 2c (0.2 m s^{-1}), we conclude that the uncertainty for the difference $[w_a - w_r]$ is about 0.22 m s^{-1}. (The uncertainty of a sum of two quantities, assumed to be independent, is the root-sum-square of the uncertainties for each quantity.)

The distribution of vertical velocities along most flight legs in the CBL is positively skewed: strong updrafts (over 2 m s^{-1}) are more common than strong downdrafts (under –2 m s^{-1}). This skewness is typical in the CBL since updrafts in thermals occupy less area than downdrafts (LeMone 1990). It results from the fact that updrafts are driven by buoyancy and downdrafts are largely compensating motion, as shown by large eddy simulations of the CBL (e.g., Mason 1989).

Even though the synoptic conditions on the three

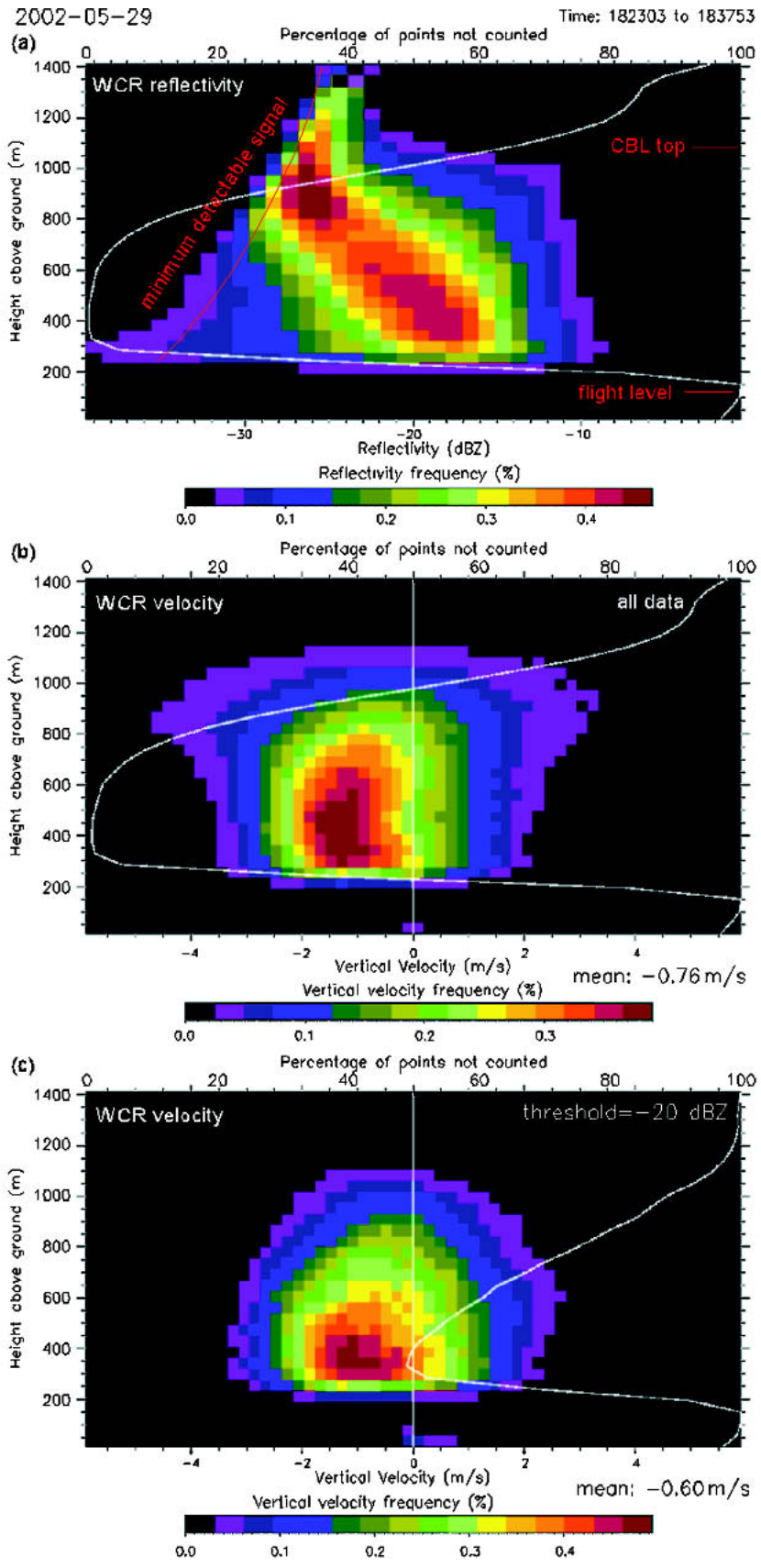
2002-05-29
Time: 182303 to 183753
(a)
Percentage of points not counted
WCR reflectivity
minimum detectable signal
CBL top
flight level
Height above ground (m)
Reflectivity (dBZ)
Reflectivity frequency (%)
(b)
WCR velocity
all data
Vertical Velocity (m/s)
mean: −0.76 m/s
Vertical velocity frequency (%)
(c)
WCR velocity
threshold=−20 dBZ
mean: −0.60 m/s

flights summarized in Table 1 were rather quiescent, some local sustained upward motion may have occurred. This motion should be less than 0.1 m s^{-1} (i.e., the true leg-mean $|w_a| < 0.1$) since none of the three days examined here experienced deep convection near the flight track. Yet, on all three days deep static instability was present and convective inhibition would be eroded if the CBL deepened 600–1100 m beyond the observed maximum depth. A sustained uplift of 0.1 m s^{-1} thus would yield deep convection in merely 1.5–3 h. Some Ekman convergence and uplift were possible on 6 and 17 June since the sea level isobars were slightly concave in the vicinity of the flight track (Fig. 2). We also looked for evidence for a thermally direct mesoscale circulation controlled by land surface conditions or topography, in view of questions raised by Worthington (2003) about the validity of a downward bias in wind profiler vertical velocities (section 1). On 29 May 2002 the ground at the southern end of the western track had high soil moisture, some standing water, and an infrared brightness temperature (measured from the 65-m flight level) ~11 K lower than the northern half of the track where the soil was dry (Fig. 4). Yet flight-level data offered no evidence of a vertical velocity differential between opposite ends of the track. The same applies for the flight on 30 May, the day with the least ambient wind (3.8 m s^{-1} on average at 65-m height), along the eastern track, which stretches from a broad valley to a ridge some 85 m higher.

3. Radar vertical velocity bias

a. Vertical velocities from gust probe and radar

The WCR data collected during IHOP 2002 enable an interpretation of the radar-derived vertical motions in the context of observed vertical air motion as measured by the gust probe. This may reveal a downward bias in the radar measurements, a bias that would unambiguously be due to downward motion of the scatterers relative to the air.

The WCR data are displaced from the aircraft, but the average value of the WCR vertical velocities at the nearest gate above and below the aircraft is centered within 20 m of the flight level. We denote the nearest-gate zenith (nadir) beam velocity as w_{r_up} (w_{r_down}) and their average as w_r. The 200-m blind zone may be argued to be rather deep for linear interpolation, but plume-scale vertical velocity cores can be seen to be rather continuous across this zone (Figs. 1 and 6). Values of w_r are calculated only for those flight legs where both up and down antennas operated and where the aircraft was at least 220 m above the ground.

Before averaging the up-antenna and down-antenna Doppler velocities (w_{r_up} and w_{r_down}), we must compare them. On average, w_{r_up} is slightly less than w_{r_down} (section 2c, Table 1). The instantaneous 30-Hz linear correlation between w_{r_up} and w_{r_down} is poor, ranging between $r = +0.12$ and $r = +0.35$ for the seven flight legs on 29 May, with an average of $r = +0.20$. Such poor correspondence is partly due to noise but it is also naturally limited by the spatial separation of 200 m, which is large in terms of CBL turbulence. In fact, at a horizontal displacement of 200 m the autocorrelation coefficient of vertical air motion (w_a) is only about 0.42 (ranging from 0.29 to 0.55 for the seven flight legs on 29 May). When the 30-Hz data are low-pass filtered to 2.5 s (0.4 Hz), which corresponds to an along-track distance of about 200 m and eliminates the high-frequency noise, the correlation between w_{r_up} and w_{r_down} is better: $r = +0.40$ on average, ranging between 0.27 and 0.58 for the same seven flight legs. This correlation, between filtered w_{r_up} and w_{r_down}, is quite close to the w_a autocorrelation at 200 m. This is consistent with our finding that the WCR Doppler spectra correspond well with the w_a spectrum at frequencies less than 2 Hz (170 m) (section 2c). Moreover, the horizontal autocorrelation and the (vertical) filtered w_{r_up} and w_{r_down} correlation tend to vary similarly for various flight legs (i.e., their leg averages are strongly correlated). In other words, the Doppler velocity correlation between the first radar gate up and the first gate down is as good as can be expected in this turbulent environment. So, it is physically meaningful to compare w_r (the mean of w_{r_up} and w_{r_down}) to w_a at flight level.

b. Vertical velocity bias in down- and updrafts

The CBL echo plumes generally contain updraft cores (Fig. 7), yet the WCR data, from both the up and down antennas, indicate that subsidence prevails. This is evident in Fig. 1 as a dominance of red colors over blue ones. Along one 29 May flight leg subsidence clearly prevails at all levels (Fig. 8b). The mean rate of subsidence (0.76 m s^{-1}) is significant: it is more than twice the uncertainty for w_{r_up} (section 2c) and about half the standard deviation of the velocity distribution (1.51 m s^{-1}, calculated based on all WCR velocities in the ± 6 m s^{-1} range). The mean subsidence that Lothon

←

FIG. 8. Frequency by altitude diagram of (a) reflectivity and (b),(c) WCR velocity for the 1823–1838 UTC flight leg on 29 May 2002. Diagram (c) is identical to (b) except that the sampling is conditional: only points whose reflectivity exceeds −20 dBZ are counted. Units are # (1 dBZ)$^{-1}$ (40 m)$^{-1}$ in (a) and # (0.2 m s^{-1})$^{-1}$ (40 m)$^{-1}$ in (b) and (c). The frequencies are normalized by the total count. The flight level is 65 m on average; hence, very few nadir beam data were collected. The white line in all images shows the percentage of the CBL not sampled. Also shown in (a) is the minimum detectable signal, which is range dependent.

TABLE 1. Summary comparison between radar and aircraft vertical motions. The averages are calculated over the straight and level flight sections where combined up/down antenna and WKA data are available, except for the mean wind speed and direction, which are based on the low-level flight legs (65 m AGL). The WCR velocity, corrected for aircraft motion, at the reflectivity maximum corresponding to the ground, is listed as w_{wcr_g}; at the first gate (120 m) below the aircraft, it is listed as w_{r_down}, and at the first gate (105 m) above the aircraft, it is w_{r_up}. The term w_r refers to the single-profile average of w_{r_down} and w_{r_up}, and w_r data are available only where the WCR operated in profiling mode. The flight legs used were flown between 1653 and 1936 UTC 29 May, between 1715 and 2247 UTC Jun 6, and between 1647 and 1957 UTC 17 Jun. Local solar noon is at 1843, 1833, and 1831 UTC for the three flights, respectively.

Day	29 May	6 Jun	17 Jun
Track	Western	Central	Eastern
No. of min	115	138	57
Mean wind direction at 65 m AGL	191°	202°	201°
Mean wind speed at 65 m AGL (m s^{-1})	4.9	5.3	7.6
Mean w_{wcr_g} (m s^{-1})	0.04	0.04	0.03
Mean w_{wcr_g} (upwind legs) (m s^{-1})	−0.22	−0.01	—
Mean w_{wcr_g} (downwind legs) (m s^{-1})	0.30	0.08	—
Mean w_a where w_r exists (m s^{-1})	−0.03	+0.02	+0.08
Fraction of time with w_r data	68%	89%	75%
Mean w_{r_up} (m s^{-1})	−0.72	−0.36	−0.39
Mean w_{r_down} (m s^{-1})	−0.59	−0.35	−0.09
Mean bias $[w_a - w_r]$ (m s^{-1})	0.61	0.40	0.30
Linear regression (based on binned w_a) **bias**=	0.54 + 0.45 w_a	0.36 + 0.50 w_a	0.17 + 0.53 w_a
Correlation coefficient (bin-mean values)	0.97	0.99	0.96

et al. (2002, their Fig. 8b) found in wind profiler velocities is smaller (0.22 m s^{-1}), but in magnitude it is also less than the standard deviation. This subsidence appears at all levels: there is no clear dependence on height within the CBL. When only the stronger echoes (>-20 dBZ) are sampled, the bulk of the radar scatterers still sink (Fig. 8c), but the average rate is less (0.60 m s^{-1} in this case). The tendency for radar vertical velocity to be negative, evident on all flight legs within the CBL, is not found in the gust probe data (Table 1), suggesting that the scatterers tend to subside relative to the ambient flow. It is not simply a radar data processing error because it is not found in the WCR data at ground level (section 2c, Table 1).

The difference $[w_a - w_r]$ is referred to as the *vertical velocity bias*. The term "bias" is defined here as an instantaneous discrepancy, but it becomes more meaningful when $[w_a - w_r]$ is averaged over many flight legs. The uncertainty of the $[w_a - w_r]$ is 0.2 m s^{-1}, as determined by the uncertainty of the w_r and w_a averages (section 2d). The w_a measurements are continuous, but part of the CBL is not sampled by the WCR (Fig. 5). The instantaneous $[w_a - w_r]$ values can be calculated only for profiles where both w_{r_up} and w_{r_down} are available, and the averages, to be discussed below, are based only on those profiles. Some 68% of the 29 May profiles in the 115 min with both up and down antennas in operation have both w_{r_up} and w_{r_down} values. The echo-free zones might correspond mostly with subsiding regions, possibly containing insect-free air entrained from above the CBL. It turns out that on average w_a in echo regions is slightly higher than w_a everywhere, but the difference is insignificant and in the noise: on the three days shown in Table 1, the mean w_a (where w_r exists) is less than 0.1 m s^{-1}. (Recall that the flight-leg mean w_a is set to zero; section 2d.) Even if w_a was significantly different in the echo-free zones, the partial sampling would not affect the bias statistics because a full array of w_a values exists for comparison against simultaneous w_r values.

Scatterplots of w_r versus w_a values at 30 Hz for a series of flight legs, or even just one, look like a dark cloud that reveals some correlation but a low regression coefficient. But they do show that w_r varies less than w_a, that is, that the slope of the linear regression is significantly less than one, for instance for a flight leg on 6 June (Fig. 9a) where it is 0.62. Values of the slope range from 0.42 to 0.63 for various flight legs on the three days listed in Table 1. For all flight legs on 29 May, 6 June, and 17 June the slopes are 0.55, 0.50, and 0.47 on average, respectively. Thus, $[w_a - w_r]$ increases with updraft strength.

The reproducibility of this departure from a 1:1 slope suggests the possibility that this is some artifact of the measuring systems or the method of correcting for aircraft motion. Independent checks have confirmed the accuracy of radar-derived velocities (Leon and Vali 2004, manuscript submitted to *J. Atmos. Oceanic Technol.*). Also, two different and entirely independent WCR velocity processing packages give essentially the same results (not shown). More convincing, perhaps, is the analysis of identical scatterplots for flight legs through a CBL filled with snow over Lake Michigan during a cold-air outbreak. An example from 19 January 2004 is shown in Fig. 9b. Some evidence for horizontal convective rolls exists in the reflectivity and velocity fields on that day, but the snow density was sufficient for WCR observations, even between rolls. Surely with upstream air temperatures about −17°C on that day, the air is insect free. Exactly the same radar configuration on the same aircraft and the same analysis tools were used. The slope of the linear regression

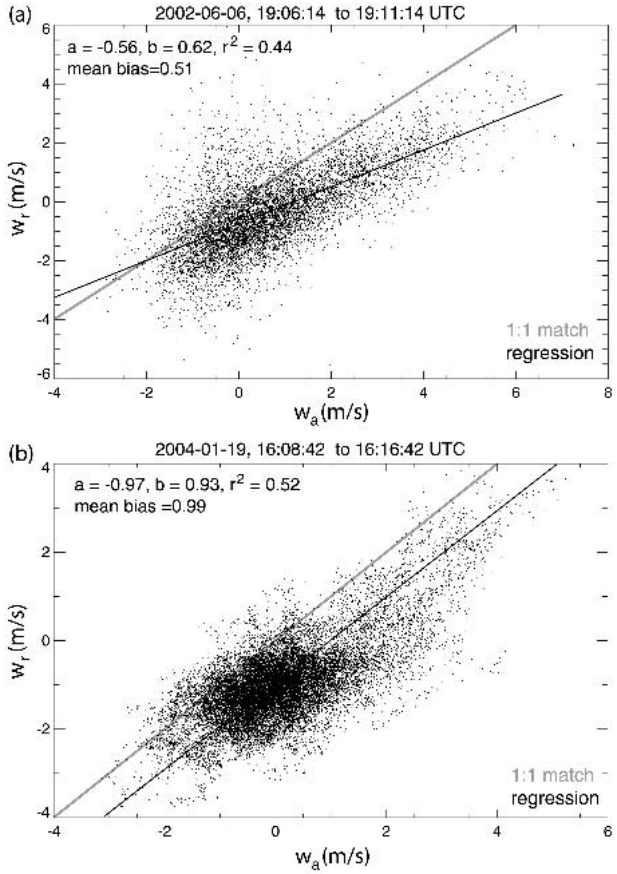

FIG. 9. Scatterplots of WCR-inferred vertical motion (w_r) vs gust probe vertical air motion (w_a) for (a) a flight leg in the optically clear CBL on 6 Jun 2002 and (b) a flight leg through a snow-filled CBL over Lake Michigan on 19 Jan 2004. Also shown are the 1:1 match line (gray), the regression line (black), the regression parameters a (intercept) and b (slope), and the mean bias $[w_a - w_r]$.

(w_r as a function of w_a) is much closer to 1.0. The average of $[w_a - w_r]$ of about 1.0 m s^{-1} is due to the fall speed of the snow crystals. In situ two-dimensional precipitation particle probe (2D-P) measurements indicate little or no riming of the snow crystals, consistent with the low concentrations of supercooled liquid water according to the forward scattering spectrometer probe (FSSP), which measures particles between 1 and 45 μm (in size), and consistent with ambient temperatures, which were near the maximum saturation vapor pressure difference between water and ice. Thus, we expect a particle fall speed of about 1.0 m s^{-1} (e.g., Fig. 3.13 of Houze 1993). In a series of cumulus congesti observed over the High Plains in July and August 2003, we also found the regression slope between w_r and w_a to be within 20% of 1.0, and a mean $[w_a - w_r]$ value consistent with the theoretical fall speed of the ice particles that are measured with the particle probes on the aircraft (not shown). Clearly the bias observed in the cloud-free CBL cannot be reproduced in clouds using the same measuring and processing methods.

The wide scatter of (w_r, w_a) points in Fig. 9 is not surprising given the spatial separation of the measurements (section 3a). To reduce the scatter we binned the w_a values in 0.2 m s^{-1} increments and calculated the mean w_r value in each w_a bin for a series of 1800 profiles. (This corresponds with a segment of 1 min or about 5 km.) Mean w_r values are shown for 115 such segments collected on the 29 May flight in Fig. 10. Clearly not all w_a bins will be equally populated. The scatter of mean w_r values broadens toward extreme values of w_a because the average w_r there is based on just a few measurements out of the total of 1800, sometimes just one. In other words the w_r values become statistically insignificant toward the tails of the w_a frequency distribution. The w_a frequency distribution is centered very close to 0 (Fig. 10) with a mean value of –0.03 m s^{-1} (Table 1). The w_a distribution is positively skewed and is very similar to that in the CBL over Lake Michigan on 19 January 2004 (Fig. 11). The same technique as that used for Fig. 10 yields a regression with a slope close to 1.0 for the flight leg shown in Fig. 11 and for other flight legs over Lake Michigan. Again, the observed difference between w_r and w_a is consistent with the terminal velocity of snow.

For updraft regions of the insect-filled CBL, $w_r < w_a$, and $[w_a - w_r]$ increases with increasing w_a (Fig. 10). For instance, in a 1 m s^{-1} updraft $[w_a - w_r]$ is 1.0 m s^{-1} on average, keeping the particles suspended, while in a 2 m s^{-1} updraft $[w_a - w_r]$ is about 1.4 m s^{-1}, according to the linear regression in Fig. 10. In other words, scatterers *tend to descend* and the *stronger the updraft*, the more *they oppose it*. In a downdraft, the bias is much smaller. That is, the opposition to updrafts increases when the air rises faster, but the bias is weaker in downdrafts (generally <0.5 m s^{-1}). Only in strong updrafts, those at least 1 m s^{-1} strong, do particles actually rise. The sample size of extremely strong updrafts is insufficient to assess whether the bias there levels off.

All w_r values for each w_a bin shown in Fig. 10 can be averaged. These average w_r values, or the corresponding bias $[w_a - w_r]$, are strongly related to w_a itself (Fig. 12). The relationship between the $[w_a - w_r]$ and w_a is linear with a correlation coefficient of 0.97 for the 29 May data (Table 1). Such high correlation clearly is affected by the scatter reduction, but the linearity is not. The binning of the independent variable (w_a) and averaging of the dependent variable (w_r) values within each w_a bin is not the same as a linear regression line. A linear regression minimizes the least squares differences between observed and regressed w_r values for all w_a values. The binning method used here separately considers different w_a values. Thus the apparent alignment of the dots in Fig. 12 is not the result of the data reduction method.

On two other days, 6 and 17 June, at different tracks (the central and eastern track, respectively; Fig. 2) a

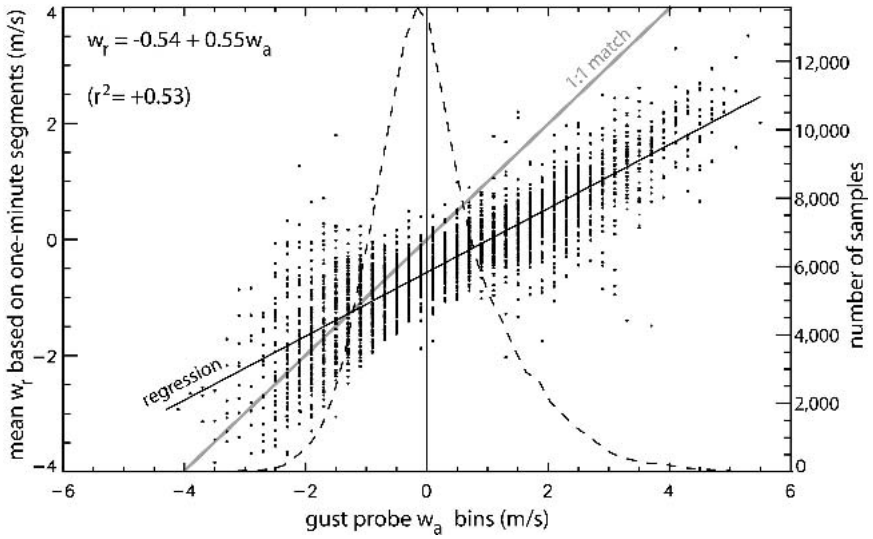

FIG. 10. WCR vertical velocity (w_r) distribution for a range of values of aircraft gust probe vertical motions (w_a), binned in 0.2 m s^{-1} increments, for 115 time segments on 29 May. Each dot represents a 1-min mean w_r value for a given w_a bin. Also shown are the linear regression equation, the correlation coefficient (r), and the distribution of adjusted w_a values (dashed line) coincident with WCR measurements.

similar relationship emerges between the average bias and w_a (Fig. 12). On these days the bias increases slightly more rapidly with increasing updraft strength, compared to 29 May, and the bias does not tend to zero in downdrafts. Consistent with the 29 May case, the bias does not display a ceiling in strong updrafts (say, $w_a >$ 2 m s^{-1}), but the small sample size of strong updrafts, also shown in Fig. 12, implies that this conclusion is not robust. The dependence of the bias on w_a, averaged over three flights (each weighted by the number of 1-min samples listed in Table 1), is given as

$$w_a - w_r = 0.49w_a + 0.42 \quad (1a)$$

or

$$w_r = -0.42 + 0.51w_a. \quad (1b)$$

The average bias for all data on three flights is 0.45 m s^{-1}. The regressions and mean bias values for the three days are listed individually in Table 1.

In short, microinsects in the CBL tend to descend, and more so in updrafts. None of the w_r versus w_a regression slopes in cloud are even close to those in the

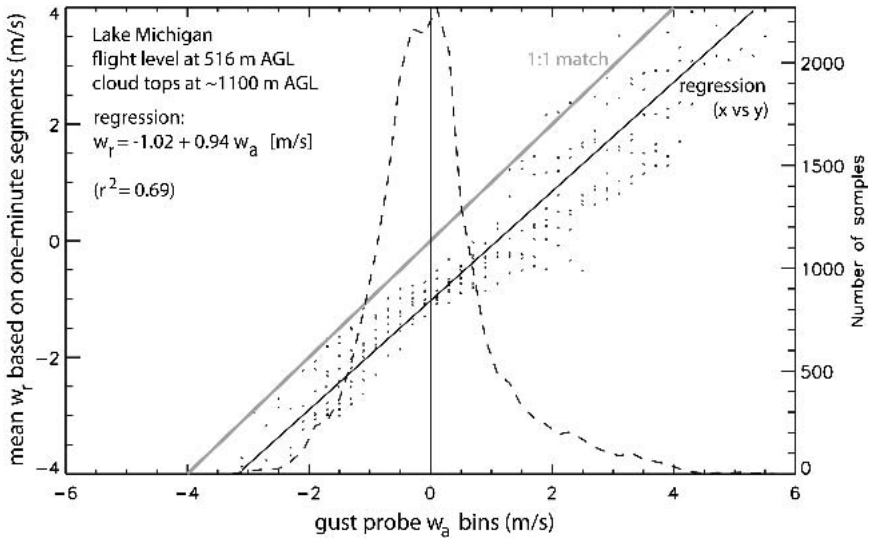

FIG. 11. As in Fig. 10 but for the same flight leg as analyzed in Fig. 9b.

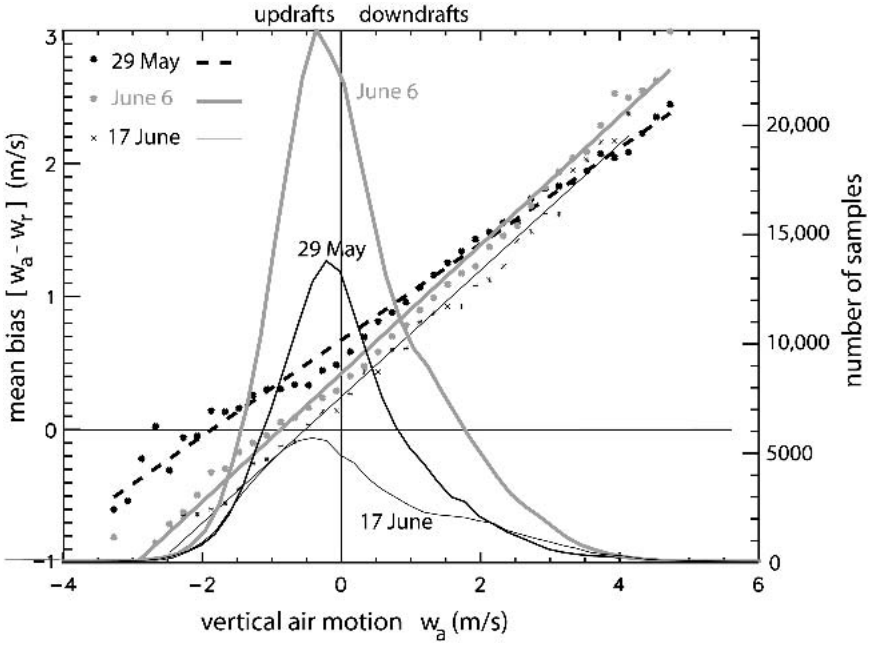

FIG. 12. Regression curves (straight lines) and observed mean bias $[w_a - w_r]$ values (dots or stars) as a function of vertical air motion w_a for three flight days and their respective distributions of adjusted w_a measurements.

clear CBL in IHOP 2002. Thus, the difference between biotic scatterers in the CBL and drops or snow in cloud is unambiguous.

To sample some stronger updrafts, we also evaluated the bias for two flight legs across a weak and mostly stationary front in the Oklahoma Panhandle in the afternoon of 3 June 2002 (not shown). The front appeared as a fine line on ground-based radar reflectivity maps. In this case the leg-mean value for w_a was not set to zero. The mean w_a for 24 one-minute time segments in the vicinity of the front was $+0.59$ m s^{-1}, and the w_a distribution was clearly skewed toward strong updrafts. The corresponding mean bias was 0.83 m s^{-1}, and the linear regression was close to the three others in Fig. 12, best matching the one for 29 May. In this case the bias did level off to about 2 m s^{-1} for very strong updrafts ($w_a > 4$ m s^{-1}), although again the sample size is too small to make a definitive statement.

c. *Variation of bias with height, echo strength, and time*

We now examine the variation of the radar vertical velocity bias with altitude within the CBL with echo strength and with the time of day. Scatterers tend to oppose updrafts a little more vigorously at low levels than in the upper CBL on 6 June (Fig. 13). The same is true on 29 May and 17 June (not shown), in which cases the low-level regression line is slightly more removed from that for the mid- and upper CBL. The larger reflectivity values in the lower CBL (Fig. 8a) are possibly the result of larger insects there, which may be able to oppose updrafts more effectively. The weak dependence of the bias on height in the CBL may be an artifact of the linear averaging of w_{r_up} and w_{r_down} across the 200-m-deep blind zone. The vertical velocity of a typical entraining thermal in the CBL tends to peak below $z_i/2$ (e.g., Fig. 5 in Noilhan and Bénech 1986). In any event, Fig. 13 shows that to first order $[w_a - w_r]$ is independent of height in the CBL. This is evident also in the full-profile frequency by altitude display of WCR velocities (Fig. 8b).

The tendency of scatterers to descend is further examined as a function of echo strength (Fig. 14). Except for the strongest echoes $[w_a - w_r]$ increases slightly with echo strength on all days. The 6 June case has more samples (Table 1) but most of the 6 June echoes are rather weak (Fig. 14), so little can be said with regard to the stronger echoes. The relationship between $[w_a - w_r]$ and echo strength on 29 May is similar to the one on 6 June (Fig. 14) but echoes tend to be stronger, so the average bias is larger than on 6 June (Table 1).

The slight increase of $[w_a - w_r]$ with echo strength does not necessarily imply that larger insects (those with a larger scattering cross section) can oppose updrafts more effectively. Echo plumes, that is, regions with rather high reflectivity values, tend to rise (Fig. 7), and therefore $[w_a - w_r]$ in the plumes may be larger, simply in response to the updraft. This explanation for the trends evident in Fig. 14 is likely, given the strong correlation between $[w_a - w_r]$ and w_a (Fig. 12), although the former explanation (related to insect size)

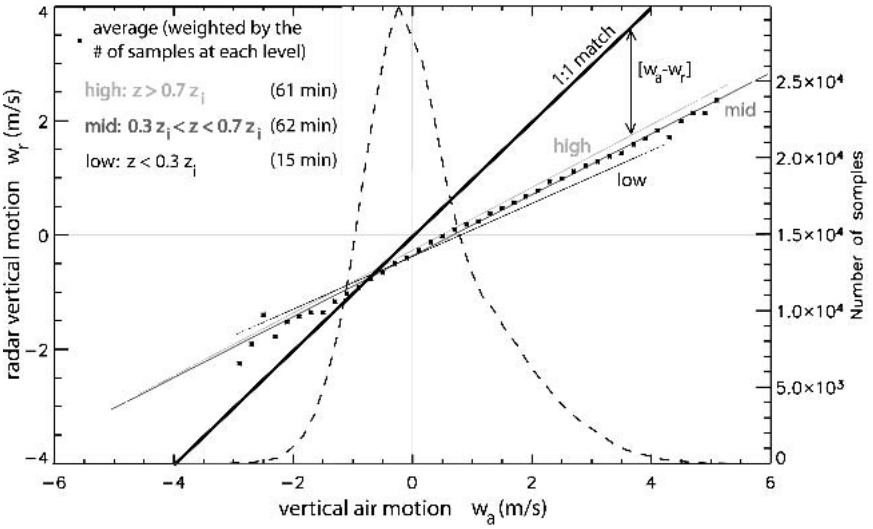

FIG. 13. Linear regressions of w_r as a function of w_a in three layers within the CBL, whose depth z_i is determined from the WCR reflectivity profile (Fig. 1). These regressions are based on 138 time segments during the 6 Jun flight. Also shown are the distribution of adjusted w_a measurements (solid curve) and the average w_r value at all levels within the CBL for each w_a bin (stars).

cannot be excluded because it is impossible to separate scattering cross section from concentration.

The bias remains positive for reflectivity values close to the minimum detectable signal (Fig. 14). Depending on range, much of the CBL undetected by the WCR (Fig. 8a) falls in this low-reflectivity region. Also noteworthy in Fig. 14 is that at high reflectivity values (>-17 dBZ) the bias seems to plateau and even decrease. This tendency should be assessed only for 29 May and 3 June, two days with strong echoes. Much variation exists but on both days the bias decreases for unusually high reflectivity values. We do not understand this trend.

In general, over the range where echoes are strong enough to exceed the minimum detectable signal and weak enough that they are not exceedingly rare in the

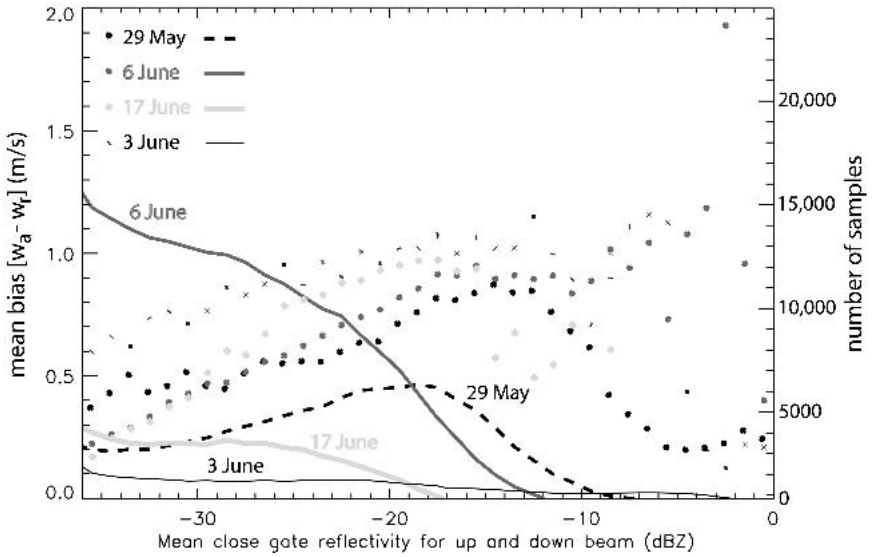

FIG. 14. Observed bias [$w_a - w_r$] values (stars) as a function of coincident radar reflectivity (binned at 1-dBZ intervals) and the distribution of reflectivity measurements (solid lines). The same three flight days as listed in Fig. 13 are shown, plus 3 Jun, a flight that focused on a frontal convergence zone.

CBL, the vertical velocity bias is a little greater in the stronger echo regions. This is evident also from Fig. 15, in which the CBL is divided into three regions according to echo strength, assuming some arbitrary reflectivity thresholds. But again, as for the effect of height in the CBL, the dependence on echo strength is rather weak.

Finally we examine the variation of $[w_a - w_r]$ as a function of time of day by means of two flight days that span over 8 h of data centered near local solar noon (LSN) (Table 2). At some 3 h, 22 min before LSN, the CBL is marginally deep enough to calculate w_r; thus the resulting regression parameters are not reliable. From some 2 h before LSN to 4 h after LSN, the slope of the regression between is near 0.5–0.6 and varies little. Both the slope and the correlation coefficient do increase slightly until the CBL is mature (Table 2). The linear regression parameters are close to the ones given in Eq. (1). The average echo strength on the last flight leg on 6 June (centered at 4 h, 10 min after LSN) was less than on the previous one and plumes were less well defined, indicating that the CBL was in decline. In short, the data in Table 2 suggest that $[w_a - w_r]$ is proportional to w_a throughout the lifetime of the continental CBL.

d. Adjusting WCR velocities

In summary, the echo vertical velocity bias relates strongly to air vertical motion, irrespective of echo strength and height in the CBL. The WCR vertical velocity profiles in the CBL then can be adjusted for best-guess echo motion. The simplest correction is a constant value (the observed mean, $+0.45$ m s^{-1}), but given the strong correlation between bias and w_a, Eq. (1) can be used to infer the best-guess vertical air velocity based on WCR data (w_{rc}) from uncorrected WCR values (w_{ru}) at any range, as follows:

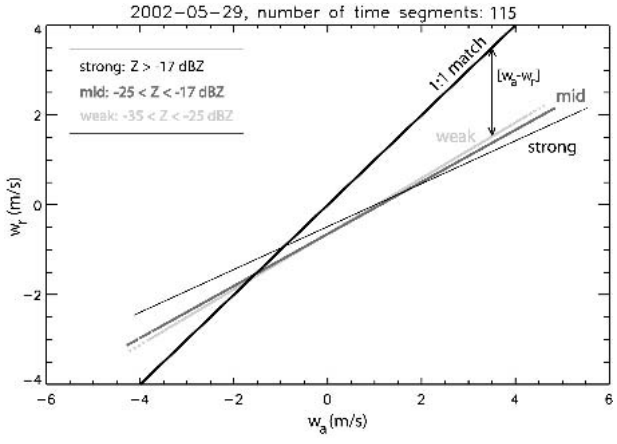

FIG. 15. The relationship between w_r and w_a stratified by echo strength for the 29 May flight.

$$w_{rc} = w_{ru} + \text{BIAS} = w_{ru} + 0.49w_a + 0.42$$
$$= 1.96(w_{ru} + 0.42) \quad (2)$$

since

$$w_a = \frac{w_{ru} + 0.42}{0.51}$$

according to Eq. (1). The adjusted WCR vertical velocity profile for the same transect shown in Fig. 1 is shown in Fig. 16. In this transect the updrafts are clearly stronger. While the average vertical motion w_{rc} in the domain is close to zero, the downdraft regions are still larger than the updraft regions in this and many other transects we examined, which implies, according to airmass continuity, that the mean rate of ascent is larger than the mean rate of subsidence. This is consistent with the observed skewness of the w_a distribution (LeMone 1990; Fig. 12).

Most echo plumes in Fig. 16 (top) appear to correspond with updrafts (blue regions in the bottom panel of Fig. 16). This is consistent with Fig. 7, a scatterplot of reflectivity versus vertical air motion. To examine this relationship more thoroughly we apply the same binning technique for w_a (Fig. 10) to reflectivity (Fig. 17) for all time segments available on 29 May and 6 June. Reflectivity values are binned at 1-dBZ intervals. Updrafts are measured in terms of w_{rc} values, locally (at the same radar gate where Z is measured), or w_a values, in the vicinity. The $Z - w_{rc}$ relationship can be assessed at any range, but only the close gates of the up and down beams are used in Fig. 17 as a way of demonstrating that the adjusted w_r values are close to the vertical air motion w_a, irrespective of reflectivity. Vertical velocities in each reflectivity bin are entirely independent of those in neighboring bins but, because numerous vertical velocity values are averaged in each reflectivity bin, some smoothness in the curves can be expected (Fig. 17). Again, as for the (w_r, w_a) plots (Fig. 12), the alignment of the points in Fig. 17 is rather surprising; clearly this is not due to the data analysis method. In any event, echo plumes tend to correspond with updrafts, or with stronger updrafts. According to Fig. 17, echo plumes (with peak reflectivity values near -10 dBZ) tend to rise at a rate of about 1.0 m s^{-1} over the background of weak echoes on both days.

The overall-mean radar vertical motion w_{rc} is less than 0.10 m s^{-1} on both 29 May and 6 June, as is the mean vertical air motion w_a. The distribution of w_{rc} (not shown) is also close to that of w_a on both days: both distributions are positively skewed although the standard deviation of w_{rc} is slightly larger than that of w_a, possibly because of the high-frequency variability of w_r, above what is expected in the CBL (section 2c).

4. Discussion

The tendency for CBL scatterers to subside relative to the air is consistent with vertical velocity averages documented by wind profilers, although the magnitude

TABLE 2. Regression parameters for $w_r = a + bw_a$ as in Eq. (1b) for various flight legs at different times. The time is expressed as hours before/after (−/+) LSN. Also shown are the mean flight level (AGL) and the WCR echo top z_{i_WCR} as defined in section 2b(1). The echo-top heights are somewhat uncertain on the first leg shown for 14 and 6 Jun because the flight level was relatively close to the CBL top, so the first gate of the zenith beam was above the lowest echo tops. Thus the values of z_{i_WCR} with a question mark are likely to present an overestimate. The 14 Jun flight legs were near the western track.

Date (Jun)	Time LSN (h:min)	Leg length (km)	Flight level (m)	z_{i_WCR} (m)	a (m s^{-1})	b	r^2
14	−3:22	34	163	297(?)	−0.15	0.30	0.02
	−2:12	48	392	692	−0.45	0.49	0.13
	−1:14	46	371	1014	−0.54	0.56	0.27
6	−1:12	51	863	1029(?)	−0.40	0.58	0.28
	+1:09	51	353	1219	−0.42	0.54	0.29
	+4:10	51	386	1105	−0.44	0.52	0.22

is somewhat larger. The average downward bias documented here (0.45 m s^{-1}) is about twice as large as that reported by Angevine (1997) and Lothon et al. (2002) (section 1). The difference may be affected by the fact that the WCR does not sample the entire CBL: net downward motion in the echo-free regions would imply a smaller overall bias. More important probably is that this study is based on three fair-weather days near the summer solstice, each with a well-developed CBL. Angevine (1997) did not exclude days with a less developed CBL, for example, windy or cloudy days, nor did he first extract those levels that were verified to fall within the CBL. Another explanation relates to the nature of the scattering: the 915-MHz return power results from both particle (insect) scattering and Bragg scattering. Bragg scattering results from air turbulence and yields an unbiased Doppler velocity. It is insignificant at 95 GHz; hence it is not surprising that the wind profilers' vertical velocity bias is smaller than the true rate of subsidence of microinsects lofted by CBL thermals.

The tendency for CBL scatterers to subside explains the absence of a vertical velocity error in nighttime wind profiler data (Angevine 1997). Many actively flying, large insects migrate at night, when the lower atmosphere is stably stratified and free of strong updrafts, which are disruptive to macroinsect migration (e.g., Richter et al. 1973; Schaefer 1976). This nocturnal migration should be essentially horizontal during most of

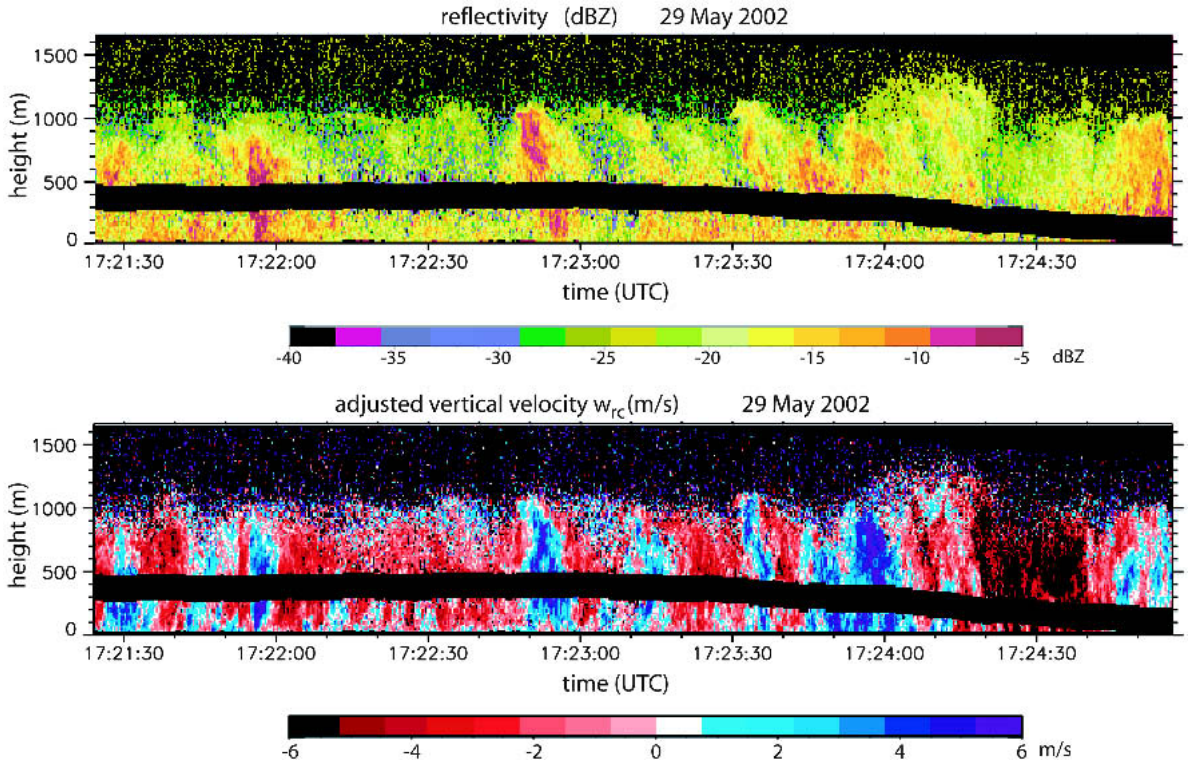

FIG. 16. As in Fig. 1 except the lower panel shows the adjusted WCR velocity w_{rc}.

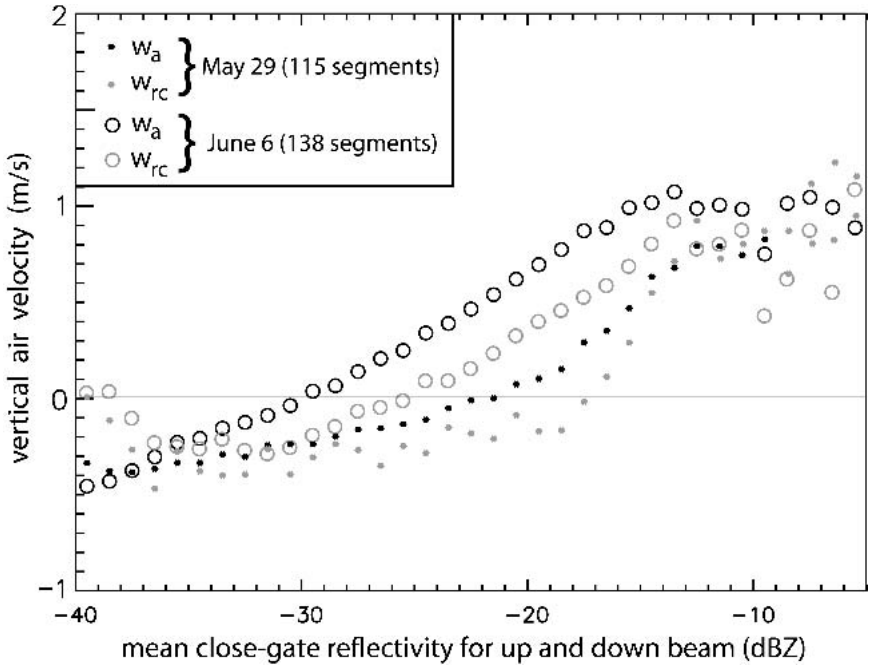

FIG. 17. Variation of adjusted WCR vertical velocity w_{rc} with radar reflectivity. Only the closest gates of the nadir and zenith beams are used. The WCR values are averaged for all time segments on two flights, as in Fig. 14. Also shown is w_a, averaged in the same way as w_{rc}.

the flight. The presence of microinsects above the surface layer appears to be a daytime phenomenon (e.g., Konrad 1970; Isard et al. 1990). WCR measurements before and shortly after dawn indicate that scatterers are virtually absent in the stable boundary layer (BL), at least in the Oklahoma Panhandle. This is confirmed by WCR data collected from 1 h before sunrise to almost 2 h after sunrise, on two different days (16 May and 4 June 2004). On both mornings a nearby S-band radar (S-POL) observed a wave train of weak fine lines. These fine lines remained essentially undetected by the WCR at close range. They were confirmed by in situ WKA data to be ridges of large-amplitude gravity waves in a highly stable layer. This observation confirms that at S band, Bragg scattering can contribute the observed echoes, as suggested by Gossard (1990).

Three other WKA flights were conducted from 1.5 h after sunrise until 1 h after local solar noon, to study the development of the CBL on mostly clear, mostly calm days in June (Weckwerth et al. 2004). These data show that shallow plumes (~100 m deep) can first be seen by the WCR about 2 h after sunrise (Fig. 6). The CBL thermals, and the echo plumes that render the thermals "visible," grow in depth during the course of the morning, pushing the CBL top higher. This explains the gradual development of a downward bias in wind profiler vertical velocities during the morning hours (Angevine 1997).

The w_a/w_r comparison yields further evidence, albeit indirect, that the CBL echoes are mostly small insects, as has been suggested (Vaughn 1985; Russell and Wilson 1997; Riley 1999). Not only these biotic scatterers try to return to the earth surface; hydrometeors or other nonflying particles, such as dust, plant material, etc., also subside. However, the latter attain an equilibrium fall speed that is a function of their density, size, and shape. The scatterers documented here do not fall at a terminal velocity. The w_a/w_r comparison indicates that, unlike hydrometeors, they do not fall at all when embedded in a downdraft: they ride weak downdrafts and fly up against stronger ones. And when microinsects encounter an updraft, they actively oppose it at a rate proportional to the updraft strength.

This finding also explains the very existence of radar fine lines in areas of sustained convergence such as at a dryline, a cold front, a sea-breeze front, an outflow boundary, a horizontal convective roll, or a topographic ridge. To explain S-band reflectivity enhancements of some 10–30 dBZ in fine lines, concentrations of insects must be much larger in these lines (Wilson et al. 1994; Russell and Wilson 1997). Conserved nonsedimenting quantities such as water vapor mixing ratio would not concentrate in thermals or fine lines; higher concentrations may be found in updrafts associated with an upward moisture flux, but the anomalies are small. Particles that fall at a constant speed can occur in the CBL as long as a local upward particle flux exists, that is, as long as the vertical air motion locally exceeds the par-

ticle fall speed. If these particles arise from the ground, then they will exist in higher concentrations in updraft regions because of upward advection.

The existence and persistence of radar fine lines and echo plumes has long been hypothesized to be due to a biotic response (e.g., Schaefer 1976; Drake and Farrow 1988). Our work confirms this hypothesis, but it questions the mechanism of this response. Radar entomologists have assumed that this response is to lower temperatures at higher altitudes. The argument is based on the fact that insects are poikilotherms (e.g., Schaefer 1976; Drake 1982; Pedgley et al. 1982; Achtemeier 1991): insects lose their ability to fly in air colder than some threshold. Achtemeier (1991) used this theory to explain the existence and persistence of the echo associated with a gust front. He suggested that the scatterers (which he believed to be mainly grasshoppers) only oppose updrafts where they encounter temperatures too low to maintain a wing beat sufficient for lift. Pedgley (1982) mentions a temperature threshold of 18°C for most insects. Symmons and Luard (1982) also assumed a temperature-dependent response in an idealized numerical simulation as a way to explain the development of high concentrations of the locust *Chortoicetes terminifera* in the vicinity of a frontal convergence zone. They assume that, as soon as the ambient air temperature falls below 20°C, *C. terminifera* descend at a speed of 0.4 m s^{-1}.

A first argument against the air temperature control theory in the cases examined here is that the temperature in the coolest CBL regions, near the CBL top, was above 17°C on all four days [29 May (Fig. 3), 3 June, 6 June, and 17 June 2002]. This implies that only a thin layer near the top of the CBL (if any) would be cool enough to invoke a flight response, because the temperature lapse rate in the CBL is 1°C/(100 m)$^{-1}$. It should be noted that the temperatures we encountered on the four flight days mentioned here are not exceptional. Thus, by extension, this argument applies to the central Great Plains in summer in general.

A second argument against the air temperature control theory is that the downward bias appears to occur at all levels within the CBL. According to the temperature control theory, the bias would only occur in the upper CBL. This is not confirmed by our findings (Fig. 13) or by profiler data (Fig. 5 in Angevine 1997; Fig. 8 in Lothon et al. 2002). In fact, in all three studies the bias is slightly larger at low levels than at upper levels in the CBL.

As a third argument, Geerts and Miao (2004, manuscript submitted to *Environ. Entomol.*) track insect concentrations in a steady-state 2D airflow field that is representative of a mature CBL. Several scenarios are considered including one in which insects oppose the updraft, according to Eq. (1), and one in which insects fall down only in the upper CBL, where the temperature is assumed to be too low. That simple computational experiment confirms that, when insects oppose updrafts, (i) their concentrations can readily exceed the background value by more than an order of magnitude in regions of sustained low-level convergence, and (ii) echo plumes tend to be collocated with updrafts. Both conditions are validated by observations presented in the current study (Figs. 1, 7, and 17). Neither condition occurs when insects fall down in response to a temperature threshold.

In short, the updraft opposition theory represents a plausible and verified alternative to the temperature control theory, at least for microinsects in the daytime CBL. We believe that the updraft opposition has an adaptive advantage (Geerts and Miao 2004, manuscript submitted to *Environ. Entomol.*): by floating down against the updraft, weakly flying insects do not diverge at the top of thermals, as do passive tracers, and thus they remain in the updraft longer and can be carried further downwind, allowing them to colonize new breeding and feeding grounds. This flight behavior probably takes far less energy than trying to remain aloft in a mix of downdrafts and updrafts. It is not clear what physiological mechanism allows the observed insect response. Possibly the insects sense air pressure, or temperature change, rather than just an absolute temperature. This question is beyond the scope of this study.

5. Conclusions

An airborne 95-GHz Doppler radar is used to examine the vertical velocity and thermodynamic characteristics of the optically clear CBL during IHOP 2002. The analysis is based mainly on synoptically quiescent conditions, but the results are likely to apply also to disturbed conditions involving fronts or other boundaries. The close-gate radar velocities, at 105 m above and 120 m below the aircraft, are compared to gust probe vertical velocities after they are corrected for aircraft motion. The accuracy of these corrections and the proximity of the antenna pointing angles to the local zenith are assessed, and this suggests that differences between the gust probe and the radar vertical velocities are accurate to 0.2 m s^{-1} or better for long-track averages. Our conclusions are as follows.

- Clear-air echoes are sufficiently strong for an airborne cloud radar to see most of the CBL, at least in the central Great Plains in late May and in June.
- The CBL reflectivity field is dominated by well-defined plumes, most of which penetrate to the CBL top. These plumes tend to be associated with updrafts.
- Scatterers in the CBL tend to subside, at an average rate of 0.5 ± 0.2 m s^{-1}, relative to the air. This rate of subsidence is largely independent of echo strength, time of day, or height in the CBL.
- The CBL scatterers tend to oppose updrafts in which they are embedded. Data from at least three different

flights in the CBL confirm that this opposition (measured as the difference between gust probe and radar vertical velocity, $[w_a - w_r]$) increases with updraft strength. Several checks argue for the validity of this finding, the main one being a comparison with hydrometeor scatterers: the latter yield a positive $[w_a - w_r]$ value due to the particle fall speed, but it is unrelated to vertical air motion.
- The ability of the scatterers to respond to updraft strength is an indication of their biotic nature. We argue that the response of microinsects to updrafts, not to decreasing temperatures in the upper CBL, explains the development of well-defined radar echo plumes in updraft regions in the, otherwise, well-mixed BL. By extension, this biotic response also explains radar "fine lines," along which deep convection tends to initiate.

It is thus recommended that 95-GHz-radar-derived vertical velocities within the optically clear continental CBL during the warm season be corrected for insect motion. Specifically, we propose that Eq. (1) is used, at least for relatively small vertical drafts. An example of such correction is shown in Fig. 16. In a follow-up study, we plan to use these results to examine the spatial dimensions of echo plumes and associated updrafts, and to determine whether they are dynamically equivalent to thermals.

Acknowledgments. This research was supported by National Science Foundation Grant ATMS0129374. Dave Leon processed the WCR radial velocities and reviewed. Sam Haimov was responsible for the WCR data collection. Rick Damiani analyzed the radar/gust probe vertical velocity relationship for the High Plains cumuli congesti. This manuscript benefited from reviews by Alistair Fraser, Tammy Weckwerth, and Margaret LeMone.

REFERENCES

Achtemeier, G. L., 1991: The use of insects as tracers for "clear-air" boundary-layer studies by Doppler radar. *J. Atmos. Oceanic Technol.,* **8,** 746–765.

Angevine, W. M., 1997: Errors in mean vertical velocities measured by boundary layer wind profilers. *J. Atmos. Oceanic Technol.,* **14,** 565–569.

Barnes, G., G. D. Emmitt, B. Brummer, M. A. LeMone, and S. Nicholls, 1980: The structure of a fair weather boundary layer based on the results of several measurement strategies. *Mon. Wea. Rev.,* **108,** 349–364.

Carter, D. A., K. S. Gage, W. L. Ecklund, W. M. Angevine, P. E. Johnston, A. C. Riddle, J. S. Wilson, and C. R. Williams, 1995: Developments in UHF lower tropospheric wind profiling at NOAA's Aeronomy Laboratory. *Radio Sci.,* **30,** 997–1001.

Clothiaux, E. E., T. P. Ackerman, G. G. Mace, K. P. Moran, R. T. Marchand, M. A. Miller, and B. E. Martner, 2000: Objective determination of cloud heights and radar reflectivities using a combination of active remote sensors at the ARM CART sites. *J. Appl. Meteor.,* **39,** 645–665.

Dean, T. J., and V. A. Drake, 2002: Properties of biotic targets observed with an X-band radar profiler and the potential for bias in winds retrieved from Doppler weather radars. *Proc. 11th Australasian Remote Sensing and Photogrammetry Conf.*, Brisbane, Queensland, Australia, Australian Institute of Remote Sensing, 698–711.

Drake, V. A., 1982: Insect in the sea-breeze front at Canberra: A radar study. *Weather,* **37,** 134–143.

——, and R. A. Farrow, 1988: The influence of atmospheric structure and motions on insect migration. *Annu. Rev. Entomol.,* **33,** 183–210.

Ecklund, W. L., D. A. Carter, and B. B. Balsley, 1988: A UHF wind profiler for the boundary layer: Brief description and initial results. *J. Atmos. Oceanic Technol.,* **5,** 432–441.

Gossard, E. E., 1990: Radar research on the atmospheric boundary layer. *Radar in Meteorology*, D. Atlas, Ed., Amer. Meteor. Soc., 477–527.

Houze, R. A., 1993: *Cloud Dynamics*. Academic Press, 573 pp.

Huaman, M. M., and B. B. Balsley, 1996: Long-term average vertical motions observed by VHF wind profilers: The effect of slight antenna-pointing inaccuracies. *J. Atmos. Oceanic Technol.,* **13,** 560–569.

Isard, S. A., M. E. Irwin, and S. E. Hollinger, 1990: Vertical distribution of aphids (*Homoptera:Aphididae*) in the planetary boundary layer. *Environ. Entomol.,* **19,** 1473–1484.

Knight, C. A., and L. J. Miller, 1993: First radar echoes from cumulus clouds. *Bull. Amer. Meteor. Soc.,* **74,** 179–188.

——, and ——, 1998: Early radar echoes from small, warm cumulus: Bragg and hydrometeor scattering. *J. Atmos. Sci.,* **55,** 2974–2992.

Koch, S. E., and C. A. Ray, 1997: Mesoanalysis of summertime convergence zones in central and eastern North Carolina. *Wea. Forecasting,* **12,** 56–77.

Konrad, T. G., 1970: The dynamics of the convective process in clear air as seen by radar. *J. Atmos. Sci.,* **27,** 1138–1147.

LeMone, M. A., 1990: Some observations of vertical velocity skewness in the convective planetary boundary layer. *J. Atmos. Sci.,* **47,** 1163–1169.

——, R. L. Grossman, F. Chen, K. Davis, and B. Geerts, 2003: The effects of surface heterogeneity on boundary-layer structure and energy fluxes from aircraft. Preprints, *Symp. on Observing and Understanding the Variability of Water in Weather and Climate*, Long Beach, CA, Amer. Meteor. Soc., CD-ROM, 1.4.

Lenschow, 1972: The measurement of air velocity and temperature using the NCAR Buffalo Aircraft Measuring system. NCAR Tech. Note NCAR-TN EDD-75, 39 pp.

Leon, D. C., A. Guyot, P. Laborie, A. Pazmany, J. Pelon, J. Testud, and G. Vali, 1999: Vertical plane velocity fields retrieved from dual-beam airborne Doppler radar data. Preprints, *29th Int. Conf. on Radar Meteorology*, Montreal, QC, Canada, Amer. Meteor. Soc., 472–475.

Lothon, M., B. Campistron, S. Jacoby-Koaly, B. Bénech, F. Lohou, and F. Girard-Ardhuin, 2002: Comparison of radar reflectivity and vertical velocity observed with a scannable C-band radar and two UHF profilers in the lower troposphere. *J. Atmos. Oceanic Technol.,* **19,** 899–910.

Martner, E. M., and K. P. Moran, 2001: Using cloud radar polarization measurements to evaluate stratus cloud and insect echoes. *J. Geophys. Res.,* **106,** 4891–4897.

Mason, P. J., 1989: Large-eddy simulation of the convective atmospheric boundary layer. *J. Atmos. Sci.,* **46,** 1492–1516.

Nastrom, G. D., and T. E. VanZandt, 1996: Biases due to gravity waves in wind profiler measurements of winds. *J. Appl. Meteor.,* **35,** 243–257.

Noilhan, J., and B. Bénech, 1986: Experimental study of an artificial thermal plume in the boundary layer. Part III: Dynamic structure within the plume. *J. Climate Appl. Meteor.,* **25,** 458–467.

Pazmany, A., R. McIntosh, R. Kelly, and G. Vali, 1994: An airborne 95 GHz dual-polarized radar for cloud studies. *IEEE Trans. Geosci. Remote Sens.,* **32,** 731–739.

Pedgley, D. E., 1982: *Windborne Pests and Diseases: Meteorology of Airborne Organisms*. Ellis Horwood, 284 pp.

——, D. R. Reynolds, J. R. Riley, and M. R. Tucker, 1982: Flying insects reveal small-scale wind systems. *Weather,* **37,** 295–306.

Ralph, F. M., 1995: Using radar-measured radial vertical velocities to distinguish precipitation scattering from clear-air scattering. *J. Atmos. Oceanic Technol.,* **12,** 257–267.

Richter, J. H., D. R. Jensen, V. R. Noonkester, J. B. Kreasky, and M. W. Stimmann, 1973: Remote radar sensing: Atmospheric structure and insects. *Science,* **180,** 1176–1178.

Riley, J. R., 1985: Radar cross section of insects. *Proc. IEEE,* **73,** 228–232.

——, 1999: Radar returns from insects: Implications for meteorological radars. Preprints, *29th Int. Conf. on Radar Meteorology*, Montreal, QC, Canada, Amer. Meteor. Soc., 390–393.

Russell, R. W., and J. W. Wilson, 1997: Radar-observed "fine lines" in the optically clear boundary layer. Reflectivity contributions from aerial plankton and its predators. *Bound.-Layer Meteor.,* **82,** 235–262.

Schaefer, G. W., 1976: Radar observations of insect flight. *Insect Flight*, R. C. Rainey, Ed., Wiley, 157–197.

Symmons, P. M., and E. J. Luard, 1982: The simulated distribution of night-flying insects in a wind convergence. *Aust. J. Zool.,* **30,** 187–198.

Syrett, W. J., B. A. Albrecht, and E. E. Clothiaux, 1995: Vertical cloud structure in a midlatitude cyclone from a 94-GHz radar. *Mon. Wea. Rev.,* **123,** 3393–3407.

Vaughn, C. R., 1985: Birds and insects as radar targets: A review. *Proc. IEEE,* **73,** 205–227.

Weckwerth, T. M., and Coauthors, 2004: An overview of the International H_2O Project (IHOP_2002) and some preliminary highlights. *Bull. Amer. Meteor. Soc.,* **85,** 253–277.

Wilson, J. W., and W. E. Schreiber, 1986: Initiation of convective storms by radar-observed boundary-layer convergent lines. *Mon. Wea. Rev.,* **114,** 2516–2536.

——, and D. L. Megenhardt, 1997: Thunderstorm initiation, organization, and lifetime associated with Florida boundary layer convergence lines. *Mon. Wea. Rev.,* **125,** 1507–1525.

——, G. B. Foote, N. A. Crook, J. C. Fankhauser, C. G. Wade, J. D. Tuttle, and C. K. Mueller, 1992: The role of boundary layer convergence zones and horizontal rolls in the initiation of thunderstorms: A case study. *Mon. Wea. Rev.,* **120,** 1785–1815.

——, T. M. Weckwerth, J. Vivekanandan, R. M. Wakimoto, and R. W. Russell, 1994: Boundary-layer clear-air radar echoes: Origin of echoes and accuracy of derived winds. *J. Atmos. Oceanic Technol.,* **11,** 1184–1206.

Worthington, R. M., 2003: Comment on "Comparison of radar reflectivity and vertical velocity observed with a scannable C-band radar and two UHF profilers in the lower troposphere." *J. Atmos. Oceanic Technol.,* **20,** 1221–1223.

——, A. Muschinski, and B. B. Balsley, 2001: Bias in mean vertical wind measured by VHF radars: Significance of radar location relative to mountains. *J. Atmos. Sci.,* **58,** 707–723.